



DELFT UNIVERSITY OF TECHNOLOGY

FACULTY OF ELECTRICAL ENGINEERING, MATHEMATICS AND
COMPUTER SCIENCE

Rotary-Encoder-Based Surgical Tool Interfacing

BSc GRADUATION PROJECT
EE3L11

BAP GROUP G.2

Authors:

Djordi Kruyt (5328640)
Julia Overbeek (5406102)
Carlijn Willems (5306972)

July 1, 2024

Abstract

This report entails the design process and development of a rotational ring system that must serve as an user interface for an existing system, the ADEPTH. The goal of the rotational ring is to allow a surgeon to make selections in the user interface system. After careful consideration of the provided list of requirements, it was decided to use changes in magnetic fields, sensed by a Hall sensor. This Hall sensor detects whether an external ring was rotated to the left or to the right. The inside of the ring contains six samarium-cobalt magnets, chosen for their extreme resistance to demagnetisation at high temperatures. This was a consideration, because the magnets have to undergo repeated cycles of sterilisation as hot as 134° C. After iterated prototype testing, a final working prototype has been developed, which can communicate wirelessly with the user interface system and send 'left' & 'right' commands. This final prototype is watertight and low power, which satisfies two of the most desired requirements.

Preface

This thesis is presented as part of the Bachelor Graduation Project from the Bachelor of Electrical Engineering at the Technical University of Delft. The project was made with close involvement from the project proposer, SLAM Orthopedic. This project was carried out by six students, divided into two subgroups. Each subgroup had the same problem statement, but tried to develop a different solution. This subgroup settled on rotary switch interface, the other subgroup chose to implement an RFID scanner.

We would like to thank our supervisor dr. Massimo Mastrangeli, who was not only closely involved but also very enthusiastic about our project. Second, we would like to thank the proposers of our project, Bart Kölling and Tijs Moree from SLAM Orthopedic. Their help with the project, the option to work at YES!Delft, and the demonstrations of the ADEPTH system made this thesis possible. Finally, we would like to give special thanks to doctors John Barker and Frédérique Meeuwsen for providing us invaluable knowledge on procedures in the operating room through interviews, and prof. dr. ir. Leon Abelmann for explaining how to simulate the magnets.

*Djordi Kruyt, Julia Overbeek, and Carlijn Willems
Delft, June 2024*

Contents

List of Figures	v
List of Tables	vi
1 Introduction	1
1.1 The ADEPTH	1
1.2 Problem statement	1
1.3 Preliminary Research	2
1.3.1 Lay-out of the Operating Room	2
1.3.2 Sterilisation	2
1.3.3 Drilling in orthopaedic surgeries	2
1.3.4 Intuitiveness	3
1.4 Possible solutions	3
1.5 Proposed solution	4
2 Program of requirements	5
2.1 Stakeholder needs	5
2.2 User requirements	5
2.3 Company requirements	5
2.4 Educational requirements	6
2.5 Technical system requirements	6
3 Design process, justification, and implementation	7
3.1 System architecture	7
3.2 The Hall effect	8
3.2.1 Hall effect sensor	9
3.3 The TLE4966L	9
3.3.1 Chopper Stabilisation	10
3.3.2 Amplifier & Schmitt Trigger	10
3.3.3 Open Collector Output Transistors & Pull-Up Resistor	10
3.4 Magnets	11
3.4.1 Intrinsic Properties	12
3.4.2 Simulation	12
3.5 Prototype 3D Design	16
3.5.1 Rapid prototyping	16
3.5.2 3D models of the prototype	17
3.5.3 Final 3D design	19
3.6 Micro controller	20
3.7 Prototyping Board	22
3.8 Wireless communication	23
3.9 Code and FSM	23
3.10 Selection mechanism	25
4 Results	26
4.1 Power usage	26
4.2 Demonstration	27
5 Discussion of results	29
6 Conclusion	30
7 Recommendation	30
References	31
Appendix	33

A Surgeon Interviews	33
A.1 Interview John Barker	33
A.2 Interview Bas de Hartog	33
B Python code for magnet simulation	36
C Magnet Simulations	42
D Arduino & Feather Code	61
D.1 Arduino code	61
D.2 Feather Code	63
D.3 Feather Receiver Code	66
E Prototype Results	69

List of Figures

1	Screws are placed in a broken bone to hold it in place[1].	1
2	A CAD model of the ADEPTH.	1
3	The ADEPTH in a demonstration[3].	1
4	Communication during a drilling procedure in an orthopaedic surgery.	3
5	System architecture block diagram for communication for the UART connection.	7
6	The Hall effect. Adapted from [15].	9
7	(a) Open collector circuit diagram. (b) TLE4966L internal architecture.	9
8	Open collector output circuit with Zener diode & pull-up resistor.	11
9	Timing definition of the speed signal with applied external magnetic field. Adapted from [21].	12
10	Simulated magnetic field with 6 dipoles. Black circle represents the ADEPTH hull. Blue arrows represent the magnetic dipoles. Red arrow represents the feedback magnet. Red dot represents the Hall sensor. Green arrows represent the magnetic field lines.	14
11	Simulated magnetic field along the x-plane of the Hall sensor for 6 dipoles versus angle. Blue waveform is the magnetic field density along the x-plane at the Hall sensor. Red waveform is the corresponding logic speed signal output of the Hall sensor, triggered at $\pm 7.5\text{mT}$	15
12	Simulated magnetic field along the y-plane of the Hall sensor for 6 dipoles versus angle.	15
13	First designs for implementation on the ADEPTH.	16
14	Dimensions of life size ADEPTH with ring in mm.	17
15	Iterations of the 3D models for prototype designs.	19
16	Final 3D model of the prototype.	19
17	Circuit of the prototype with the Arduino.	20
18	Prototype of the breadboard with Hall sensor.	20
19	Pull-up electric circuit of the micro controller.	21
20	Waveform received at the micro controller.	21
21	Prototyping board with Arduino.	22
22	First complete prototype and a close up of the magnetic ring.	22
23	Communication block diagram for the wireless connection.	23
24	Prototype with Feather board.	23
25	Waveform with states changes.	24
26	FSM.	24
27	Prototype with button.	25
28	Test set up for the power usage measurements.	26
29	Demonstration of the selection method.	28
30	The final prototype.	28
31	Simulated magnetic field with 1 dipole.	42
32	Simulated magnetic field along the x-plane of the Hall sensor for 1 dipole versus angle.	43
33	Simulated magnetic field along the y-plane of the Hall sensor for 1 dipole versus angle.	43
34	Simulated magnetic field with 2 dipoles.	44
35	Simulated magnetic field along the x-plane of the Hall sensor for 2 dipoles versus angle.	44
36	Simulated magnetic field along the y-plane of the Hall sensor for 2 dipoles versus angle.	45
37	Simulated magnetic field with 3 dipoles.	45
38	Simulated magnetic field along the x-plane of the Hall sensor for 3 dipoles versus angle.	46
39	Simulated magnetic field along the y-plane of the Hall sensor for 3 dipoles versus angle.	46
40	Simulated magnetic field with 4 dipoles.	47
41	Simulated magnetic field along the x-plane of the Hall sensor for 4 dipoles versus angle.	47
42	Simulated magnetic field along the y-plane of the Hall sensor for 4 dipoles versus angle.	48

43	Simulated magnetic field with 5 dipoles.	48
44	Simulated magnetic field along the x-plane of the Hall sensor for 5 dipoles versus angle.	49
45	Simulated magnetic field along the y-plane of the Hall sensor for 5 dipoles versus angle.	49
46	Simulated magnetic field with 6 dipoles.	50
47	Simulated magnetic field along the x-plane of the Hall sensor for 6 dipoles versus angle.	50
48	Simulated magnetic field along the y-plane of the Hall sensor for 6 dipoles versus angle.	51
49	Simulated magnetic field with 7 dipoles.	51
50	Simulated magnetic field along the x-plane of the Hall sensor for 7 dipoles versus angle.	52
51	Simulated magnetic field along the y-plane of the Hall sensor for 7 dipoles versus angle.	52
52	Simulated magnetic field with 8 dipoles.	53
53	Simulated magnetic field along the x-plane of the Hall sensor for 8 dipoles versus angle.	53
54	Simulated magnetic field along the y-plane of the Hall sensor for 8 dipoles versus angle.	54
55	Simulated magnetic field with 9 dipoles.	54
56	Simulated magnetic field along the x-plane of the Hall sensor for 9 dipoles versus angle.	55
57	Simulated magnetic field along the y-plane of the Hall sensor for 9 dipoles versus angle.	55
58	Simulated magnetic field with 10 dipoles.	56
59	Simulated magnetic field along the x-plane of the Hall sensor for 10 dipoles versus angle.	56
60	Simulated magnetic field along the y-plane of the Hall sensor for 10 dipoles versus angle.	57
61	Simulated magnetic field with 11 dipoles.	57
62	Simulated magnetic field along the x-plane of the Hall sensor for 11 dipoles versus angle.	58
63	Simulated magnetic field along the y-plane of the Hall sensor for 11 dipoles versus angle.	58
64	Simulated magnetic field with 12 dipoles.	59
65	Simulated magnetic field along the x-plane of the Hall sensor for 12 dipoles versus angle.	59
66	Simulated magnetic field along the y-plane of the Hall sensor for 12 dipoles versus angle.	60
67	Demonstration on how the rotary switch would be used during an operation.	71

List of Tables

1	Chopper Frequency Noise.	10
2	Power usage.	26
3	Realised requirements for the prototype.	27

1 Introduction

During Plate Osteosynthesis, metal plates are fixed to the bone with screws to properly heal broken bones, an example can be seen in Figure 1 [1]. To ensure the proper functioning of the screws and plates, the screws have to be of the right length. This length can be determined by the depth of the hole drilled by the surgeon. To determine the depth of the hole, SLAM Orthopedic made a product called the ADEPTH [2].



Figure 1: Screws are placed in a broken bone to hold it in place[1].

1.1 The ADEPTH

The ADEPTH is an innovative device that is added to the drill and fits in between the drill and the drill bit. The ADEPTH automatically measures the total distance drilled and the length of the screw needed. In order to determine the exact screw length, the ADEPTH needs to know the diameter and type of the screw before drilling. Together with the measured rotation speed, pressure and distance to the bone, the ADEPTH can calculate the precise screw length. This information is sent to the second part of the ADEPTH system called the bridge which displays the required length on a touchscreen. Currently, this touch screen is being used to show and select the screw type, this can be seen in Figure 3 [3].

1.2 Problem statement

SLAM aims to transition to using the overhead, non-touch screens already available in operating rooms. By doing so, SLAM can provide the ADEPTH as a standalone product to hospitals, eliminating the need to supply an additional screen to already crowded operating rooms.

This brings us to the purpose of this thesis: developing an alternative screw selection mechanism for the ADEPTH to replace the touchscreen.



Figure 2: A CAD model of the ADEPTH.



Figure 3: The ADEPTH in a demonstration[3].

1.3 Preliminary Research

Before a prototype can be designed, it is important to be aware of the limitations related to a hospital environment. This section will give a brief overview of important aspects to keep in mind during design: the structure of the operating room, sterilisation, drilling and intuitiveness.

The following acronyms will be used:

CA: Circulating Assistant

OR: Operating Room

OS: Operating Surgeon

SA: Sterile Assistant

1.3.1 Lay-out of the Operating Room

An orthopaedic OR consists of a sterile and non-sterile zone; the operating surgeon (OS) and the sterile assistant(s) (SA) are in the sterile zone. There are usually between 3 and 10 people present in an OR, of which 2 to 5 are sterile [4]. It is incredibly important that people do not switch between zones, as that severely increases the risk of infection in the patient. The instruments/tools used during the operation are placed in the sterile zone close to the SA. Everyone in the sterile zone is scrubbed (cleaned) and has protective, sterile, clothing to prevent contamination [5]. The screws used during the operation are stored in the non-sterile zone and are handed to the OS or SA by the CA, see Figure 4. Each time a new instrument is needed, the OS communicates this with the SA. This means that the instruments are constantly switched between the OS and SA and must also not leave the sterile zone.

1.3.2 Sterilisation

Sterilisation is critical in orthopaedic surgeries, where infections in the bone can be fatal to the patient. For this reason, all equipment is placed in metal racks and sterilised in a high-speed pre-vacuum steamer for five minutes, using steam with a temperature of around 134° C [6]. All equipment that will be sterilised must be able to withstand the vacuum and high temperature for the required time. Different cycles can be used for sterilisation [7]; some cycles don't pull the chamber vacuum, but instead frequently change between 33 and 30 PSIA. Because of this, the sterilised items deteriorate; for example, the ADAPTH only guarantees 20 uses per device. The sterilisation damages the sensors and internal equipment and their accuracy is no longer guaranteed after 20 sterilisation.

1.3.3 Drilling in orthopaedic surgeries

In orthopaedic surgery, plates are used to stabilise fractured bones and are available in various sizes. The type of screw required can vary depending on the situation. To place these screws a hole has to be pre-drilled. During drilling, drill guides are placed on the bone to keep the drill stable. The most common types of screws used are:

- Cortical
- Locking
- Variable Angle (VA)

Concluding from the datasheet of plates given by SLAM Orthopedic [1], each type of screw uses a different guide: a locking screw uses a guide that secures it to the plate, while a cortical screw employs a guide with a handle to adjust the angle. Variable angle screws (VA screws) utilise a specialised guide that allows adjustment to various angles within the plate. Switching between different kinds of screws occurs frequently, the procedure for this can be seen in Figure 4. In practice, the correct guide is not always used for the screw type that is being placed. Sometimes, the procedure differs from the standard approach [8].

According to orthopaedic surgeon de Hartog [8], the drilling procedure starts with the SA switching to the correct drill bit onto the drill. Subsequently, it needs to be known for what screw type will be drilled, since the measurement of the ADEPTH depends on that. The drill and the drill guide

will be handed over to the OS, who will drill the hole. With the measurement from the ADEPTH, the surgeon will ask the CA and the SA for the correct screw length, of the previously chosen type. Then, the drill will be passed back to the SA, who will switch the drill bit for a screw bit. The SA also receives the sterilised screw of the correct length and type from the CA. Both of these will be passed to the OS, who will screw in the screw with the drill. After the screw has been secured in place by the OS, the drill will be handed back to the SA. Now, this cycle can be repeated until all the different screws have been placed [8].

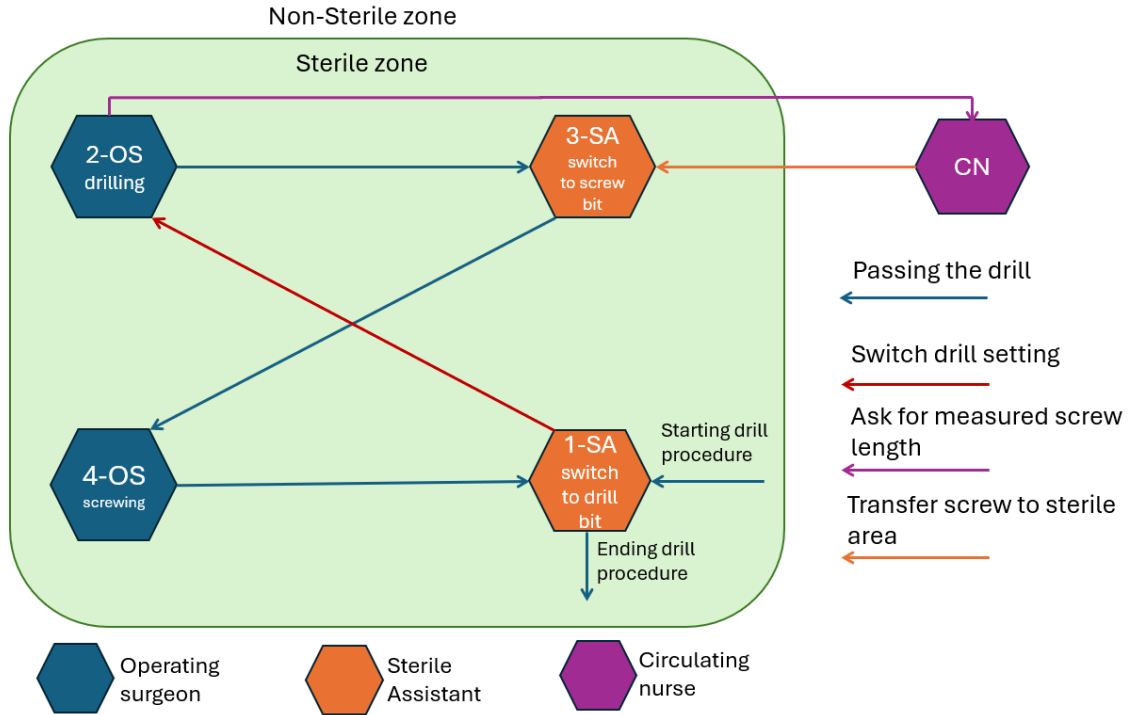


Figure 4: Communication during a drilling procedure in an orthopaedic surgery.

When looking at this procedure, it can be seen that either the SA or the OS can select the to-be-used screw type for the ADEPTH. This can be done after the SA places the correct drill bit on the drill. The CA should not be considered an option to select the screw type, because they are not involved enough in the surgery to know which screw type is used. If the CA has to select the screw types, the chances of human errors will most likely increase, which is undesirable. This is something that needs to be taken into account when designing a solution for the problem.

1.3.4 Intuitiveness

In an interview with plastic and orthopaedic surgeon John Barker (Appendix A.1), it became apparent that any new addition to a surgical procedure must be intuitive and simple to use. Surgeons are trained to follow specific methods and procedures, and, therefore, changing their established ways of working can be challenging. Thus, a good solution would be simple, intuitive, and user-friendly.

It became evident from the interviews with Doctors Barker and de Hartog (Appendix: A.1 & A.2) that each surgeon has distinct preferences for handling procedures. Doctor Barker prefers to manage tasks himself, whereas Doctor de Hartog wants the assistant to preset everything, allowing him to focus without interruptions. From the interviews, it was concluded that both the OS and the SA should be able to use the solution.

1.4 Possible solutions

In order to solve the problem of developing an alternative screw selection mechanism for the ADEPTH to replace the touchscreen, it is important to stay open to all possible solutions. The

research from the previous section has led to specific design limitations and recommendations. A key limitation is that the to be developed selection mechanism must be exclusively used in either the sterile or non-sterile part of the OR, not both. The decision was made to place it in the sterile area, as it would be operated by the operating surgeon and surgical assistant. This necessitates the product's ability to withstand sterilisation processes involving high temperatures, vacuum environments and water resistance. The primary design recommendations focus on intuitiveness, ergonomics and minimal disruption to the surgeon's existing workflow. Intuitiveness and ergonomics are crucial as they significantly affect the tool's effectiveness, error rates and user comfort. The emphasis on practicality is vital, as the surgeon might reject a tool that is not user-friendly.

The following potential solutions were evaluated:

- ID tracking - Using RFID (Radio Frequency Identification) or barcodes to identify tools and automatically apply the correct settings, ensuring efficiency and reducing manual input errors[9][10].
- Macropad - A sterilisable mini keyboard or a wrist-worn device that enables the selection of screw types directly within the sterile field, enhancing workflow efficiency[11].
- Foot pedals - Foot-operated controls to select screw types, though potentially prone to errors and ergonomic issues[12].
- Hand gestures - Utilising cameras or sensors to detect non-contact hand gestures for tool selection, although accuracy may be affected by lighting conditions[13].
- Rotary encoding - Implementing a rotary switch or hall sensors on the ADEPTH for tool selection, offering a reliable and intuitive solution, albeit with potential sealing challenges for mechanical switches.

1.5 Proposed solution

After considering all options against the design constraints and recommendations, barcode scanning, foot pedals and hand gestures were eliminated from consideration due to their impracticality for surgical use. Additionally, the macropad was discarded since it requires additional hardware and is difficult to sterilise effectively. RFID and rotary encoding emerged as the most promising replacements for the touchscreen. Since the OS and the SA alternate in using the drill, it is most convenient to integrate the solution in that step. This keeps the chosen solutions intuitive in use and easy to integrate into the existing ADEPTH system and workflow of the OS and SA. This thesis will focus on the implementation of a rotary encoding selection method.

2 Program of requirements

Now that the problem has been clearly defined, the requirements can be set in cooperation with SLAM Orthopedics. These are divided into the requirements of the users of the device, the company who produces the device, the educational requirements for the graduation project, and finally the technical aspects of the entire system. The requirements defined in the following subsections are the only requirements that need to be taken into account for this graduation project, all others are out of scope.

2.1 Stakeholder needs

In this project, a distinction is made between 'The System' and 'The Prototype Design' due to the time constraints of the bachelor's graduation project.

- The System is the solution that should satisfy all requirements.
- The Prototype Design is the prototype being developed in this project as a Proof-of-Concept, it should only satisfy 'The Prototype' requirements, not the requirements outlined for 'The System'.

2.2 User requirements

Functionality:

- The system shall select the correct screw during Plate Osteosynthesis procedures.
- The system shall require no input, or be controlled by the surgeon and/or the sterile assistant.
- The system shall be easy to use in the established workflow of the operating room.
- The system shall be intuitive to use for the user, and ergonomic.

2.3 Company requirements

System requirements:

- The system shall integrate into the existing ADEPTH design by providing input to the ADEPTH Software.
- The system shall not reduce the battery life of the ADEPTH Sensor by more than 25%, for a battery of 250mAh.
- The system should not use more than 500mA, for a pulse of 15s.
- The system should not use more than 62.5mA when on standby.
- The system shall not compromise the air- and water-tightness of the ADEPTH Sensor.
- The system shall be resistant to reprocessing by steam autoclave sterilization.
- The system shall be reusable for 20 reprocessing cycles before breakdown of any kind occurs.

Prototype requirements:

- The prototype design shall be used to demonstrate the functionality of the final system in a simulated environment using either the ADEPTH software or an Arduino.
- The prototype design does not have to fully comply with the system requirements, but the system requirements should be achievable in further iterations of the prototype design.
- The prototype shall provide input to the ADEPTH Software through a separate data channel using one of the following methods:
 - Wired Serial (UART) signal to USB input; if UART is used, the data should be sent to the 'Bridge'.
 - 868 MHz ISM data command.
 - Bluetooth Low Energy 1.

2.4 Educational requirements

- The focus should be on the electrical engineering design, and not on the materials or aesthetic design.

2.5 Technical system requirements

Functionality, Constraints (power, size, environmental factors, cost), External Interfaces

Must have:

- The prototype should use less than 12V.
- The system should use either 1.8, 3.3, or 5V.
- The system should not use more than 500mA, for a pulse of 15s.
- The system should not use more than 62.5mA when on standby.
- The part of the solution inside the ADEPTH should be smaller than the inside diameter of 38mm.
- The modified ADEPTH should not exceed a diameter of 60mm for The System.
- The prototype model of the ADEPTH, including any external components, has no diameter limit.
- The additional hardware of the prototype should be able to withstand 134°C.
- The whole system model should be able to withstand 134°C.

Could have:

- The prototype could have an option to re-select the screw type after drilling.
- The exact placement of additional hardware within the ADEPTH could be exact.
- The prototype could be integrated into the existing ADEPTH.

Won't have:

- The prototype will not concern itself with the material used in the casing, and whether that material will survive the sterilisation process.
- The prototype will not take into account a newer version of the ADEPTH.
- Neither the prototype, nor the system has to exclusively use off the shelf components.

3 Design process, justification, and implementation

An intuitive solution to scroll through the respective selection of the screw-type options present onscreen could involve a rotational selector on the ADEPTH, which is an already known application for making selections. For example, a standard drill with a torque control ring has the ability to select the torque applied by the drill. Following the interviews with orthopaedic surgeons Barker and De Hartog (Appendices subsection A.1 & subsection A.2), there is a preference for this approach, noting it as a minor yet integral step in the workflow. Since the sterile assistant is already changing drill bits, rotating a disk or ring on the ADEPTH would be a convenient addition. This idea can be implemented on the ADEPTH by using a rotary switch, such as a rotary encoder, Hall sensors, or magnetoresistive sensors.

A physical rotary switch can be used to switch between different modes. This approach has the benefit of being familiar to most people as a method for selecting a specific setting, making it an intuitive design choice. Avoiding the need to learn a new, possibly complicated selection process also decreases the existing threshold of implementing a new step into the existing workflow in the operating room. Another benefit of mechanical switching is that it can be made robust and reliable, decreasing both the probability of breaking during an operation and time needed to repair the device.

A rotary switch also has its drawbacks: using a mechanical switch means that connected parts are rotating, possibly through a brush contact, which could make achieving and maintaining a watertight seal difficult. A way to achieve water tightness is to use sensors that detect magnetic changes, like Hall- or magnetoresistive sensors. This way, the benefits of an intuitive design that is robust and reliable still remain. These sensors can be placed inside the ADEPTH, while a rotating ring of magnets can be installed on the outside. The advantage of this adaptation is that it is watertight, as there is no physical contact between any of the parts on the inside and the outside of the ADEPTH. A possible disadvantage is that unwanted, external magnetic fields may trigger the sensors in an unintended way. These fields could be generated by other electronics, the PCB present in the ADEPTH, or medical devices in the operating room

3.1 System architecture

After careful consideration, a system where a Hall sensor is placed into the ADEPTH with a rotating ring containing magnets on the outside of the ADEPTH was chosen. By rotating the ring with magnets, the Hall sensor detects speed & direction and scrolls through the respective selection of the screw-type options present onscreen. The scroll information is transmitted to the interface software via a UART connection, as illustrated in Figure 5. Figure 5 shows how the prototype would communicate with the already existing devices. The final system architecture should be wireless, and have the selection mechanism inside of the ADEPTH.

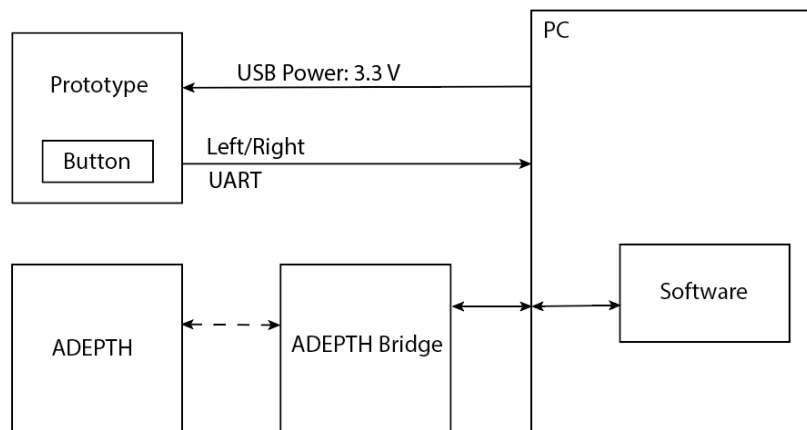


Figure 5: System architecture block diagram for communication for the UART connection.

3.2 The Hall effect

One way of detecting changes in a magnetic field is with a Hall effect sensor. A Hall effect sensor applies a fixed DC current across a thin strip of metal or wire along one axis, while measuring the potential difference (Hall voltage) along another axis. This potential difference is proportional to the axial component of the magnetic field which is perpendicular to both the current's axis and the sensing electrodes' axis [14]. The Hall effect is a consequence of the forces that are exerted on moving charges by electric and magnetic fields. The force on a moving particle with charge q is given by $F = qv \times B$, where the cross product is taken between velocity and magnetic field such that the force is perpendicular to both the velocity and magnetic field[15].

Figure 6 illustrates the Hall effect. A magnetic field is placed perpendicular to a semiconductor with current I_x . Electrons and holes flowing in the semiconductor experience a Lorentz force curving them in the -y direction. Thus, positive or negative charge accumulates on the $y = 0$ surface of the semiconductor, depending on whether the semiconductor is p-type or n-type doped, respectively. This accumulated charge induces an equal and opposite charge on the other surface resulting in a net charge, which in turn induces an electric field in the y-plane. In steady state, the force of the magnetic field will be perfectly balanced by the induced electric field force, opposing the accumulation of further charge[15][16]. This balance may be written as Equation 1.

$$F = q[E + v \times B] = 0 \quad (1)$$

which may be rewritten as Equation 2.

$$qE_y = qv_x B_z \quad (2)$$

The induced electric field E_y is the Hall field. The Hall field produces a voltage across the conductor, which is aptly named the Hall voltage. The Hall voltage can be written as Equation 3, where E_H is assumed positive in the +y direction, and V_H is assumed positive with the polarity shown in Figure 6[15].

$$V_H = +E_H W \quad (3)$$

In a p-type semiconductor, in which holes are the majority carriers, the Hall voltage will be positive. In an n-type semiconductor, in which electrons are the majority carriers, the Hall voltage will be negative[15].

The Hall voltage may also be written as Equation 4.

$$V_H = \frac{I_x B_z}{epd} \equiv -\frac{I_x B_z}{end} \quad (4)$$

Where n & p are, respectively, the electron and hole charge carrier densities, d the thickness of the conductor, and e the elementary charge[15]. As the current and applied magnetic field strength are typically small in magnitude, the Hall voltage calculated in Equation 4 is usually very small, and requires amplification in most real world applications[14]. Often, a voltage regulator is added in addition to the amplifier, to allow operation over a wide range of supply voltages[17].

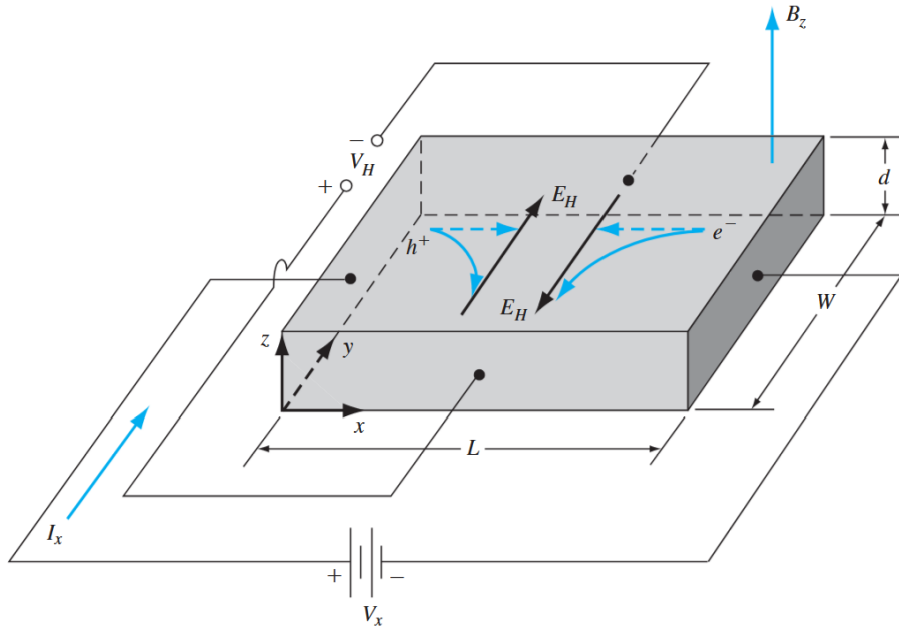
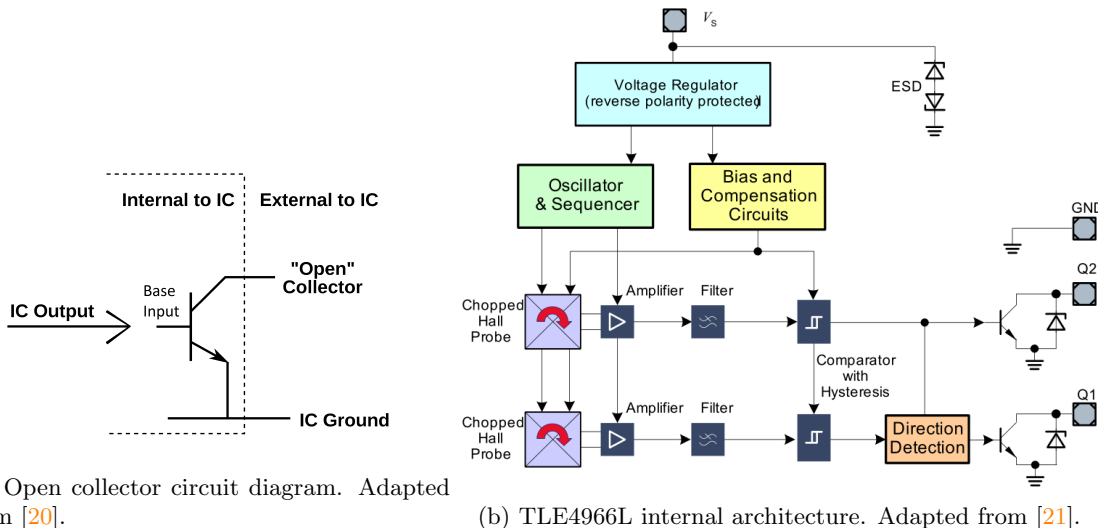


Figure 6: The Hall effect. Adapted from [15].

3.2.1 Hall effect sensor

It is sometimes desirable to have a clean digital output which is robust against noise. While the Hall element is an analog device, threshold detection circuitry can be incorporated to form an electronic switch, which outputs a binary digital signal[17]. This signal can be generated by using an open collector transistor as output: rather than producing a Hall sensor voltage at the signal output wire, it turns an output transistor on or off, providing a circuit to ground through the signal output wire[18]. This can be seen in Figure 7a. The transistor is operated between its cut-off (OFF) and saturation (ON) regions. The transistor does not operate as an amplifying device, as it would do if controlled in its active region[19].



(a) Open collector circuit diagram. Adapted from [20].

(b) TLE4966L internal architecture. Adapted from [21].

Figure 7: (a) Open collector circuit diagram. (b) TLE4966L internal architecture.

3.3 The TLE4966L

Figure 7b shows the block diagram of the chosen Hall sensor for this project, the TLE4966L[21]. Here, the output pins for the direction and speed signals, Q1 and Q2 respectively, are connected to open collector output transistors.

3.3.1 Chopper Stabilisation

The Hall effect sensor uses chopped Hall probes, which use chopper stabilisation to correct offset present at the output. This has to be done because the Hall effect element is sensitive to both magnetic fields, and to mechanical stresses put on the element. These mechanical stresses can come from molding the element into its IC Package, bending the leads, heating the chip, or from pressure being put on the sensor face. Chopper stabilisation is a switching technique that sends current in one direction of the Hall bridge and measures the output, then sends current in the other direction and measures the output again, and averages these two outputs. The result corrects for the error that comes from any mechanical stresses[22].

The switching of the current occurs at the Chopper Switching Frequency[21], during which the outputs have to be turned off. The outputs are updated at the end of each cycle. A potential problem with chopper stabilisation is that, with an instantaneous change in the magnetic field, the output may take up to $1/(\text{chopper frequency})$ to update. This has to be taken into consideration, as it can introduce significant noise for high speed applications. The chopper frequency of the chosen sensor is 320kHz, which means that the output will take up to $3.125\mu\text{s}$ to change. The maximum switching frequency is 15kHz, leading to maximum noise percentage of 4.48%, as can be observed in Table 1. Because the rotating ring with magnets will be operated by a human, it can be argued that the maximum operating frequency of the device will be below (two times the number of magnets in the rotating ring)Hz. With at most 8 magnets present in the ring, as will be justified in subsection 3.4, the operating frequency will be below 16Hz. The noise error due to chopper switching is so close to zero, as can be observed in Table 1, that it can be neglected.

Pulse Freq. (Hz)	3.125 μs Noise Percentage
15k	4.48%
16	$5 \cdot 10^{-3}\%$

Table 1: Chopper Frequency Noise.

3.3.2 Amplifier & Schmitt Trigger

As previously mentioned, the Hall voltage at the output of the chopped Hall probe is very small and needs to be amplified using a high quality DC amplifier. Afterwards, the unwanted, high frequency components are filtered out using a low-pass filter. Finally, the signal is fed to a comparator with hysteresis, a Schmitt-trigger, which provides a clean transition from off to on without contact bounce, once the applied magnetic flux density exceeds a certain limit. Built-in hysteresis eliminates oscillation by introducing a magnetic dead zone, where the switching action is disabled when the threshold value is passed[17].

3.3.3 Open Collector Output Transistors & Pull-Up Resistor

The high or low voltage outputs of the Schmitt-triggers are sent to the bases of the output transistors, setting the base-emitter voltages above or below the necessary 0.7V to turn the transistors on or off. In Figure 8 can be observed that a Zener diode is connected in parallel to the transistor's ground and output pins to protect the transistor against over-voltage. This is very useful when driving an inductive load, which can generate extremely high-voltages when current flow is suddenly interrupted or brought down to zero in a short time span.

Due to the emitter being connected to ground, the transistor either forms a short-circuit to ground when it is in its ON state; or an open circuit when the transistor is in its OFF state. To use this setup as a logic circuit, typically an external pull-up or pull-down resistor is required. This resistor sets the output voltage to high or low, respectively, when the transistor is off. This ensures that the output voltage is not left floating[18]. The output voltage V_{out} can be calculated for both transistor states by defining V_{R_L} as the voltage drop over the pull-up resistor, and solving the circuits. As a side note, because the circuit is not driving an inductive nor active load, the Zener diode can be omitted in the following calculations.

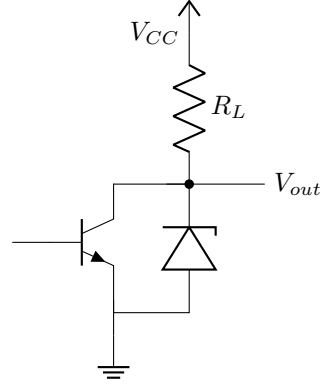


Figure 8: Open collector output circuit with Zener diode & pull-up resistor.

For both states, V_{out} can be calculated using Equation 5.

$$V_{out} = V_{CC} - V_{R_L} \quad (5)$$

For the ON State:

The transistor operates in saturation mode and makes a direct path to ground, completing the circuit. The transistor can be modeled as a short, connecting V_{out} directly to ground, setting the output voltage to 0V; a logical low.

It can be reasoned that if the transistor is on, there is a voltage drop of the supply rail voltage over the pull-up resistor, leading to a power dissipation in the resistor of

$$P_L = \frac{V_{R_L}^2}{R_L} \quad (6)$$

For the OFF State:

The transistor operates in cut-off mode and can be modeled as an open, breaking the circuit path. Because there is no closed loop, no current will flow through the circuit. The voltage drop over the pull-up resistor, V_{R_L} , is zero. This means that if the transistor is off, there is no power dissipation in the circuit, and V_{out} is equal to V_{CC} ; a logical high.

In conclusion, the output voltage is the logical opposite of the transistor state: it is high when the transistor is off, and low when the transistor is on.

3.4 Magnets

To make use of the Hall sensor, an external magnetic field needs to be applied. Therefore, appropriate magnets need to be chosen that can deliver enough magnetic flux density to switch the Hall sensor outputs. According to the datasheet of the Hall sensor[21], the minimal magnetic flux density needed to operate are specified by its operating point B_{OP} , and release point B_{RP} . The corresponding influence on the speed signal can be observed in Figure 9.

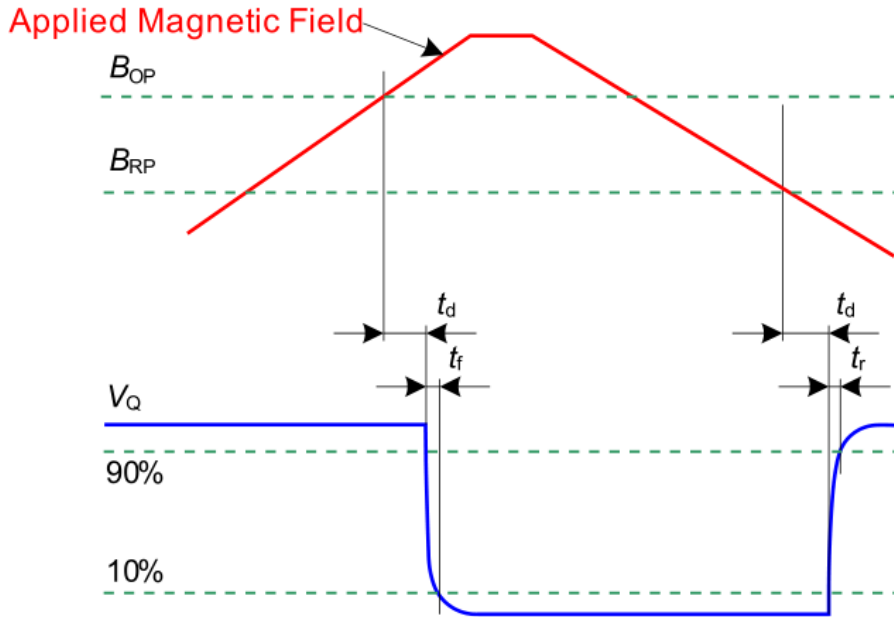


Figure 9: Timing definition of the speed signal with applied external magnetic field. Adapted from [21].

The operating point ranges from 4.7 to 10.3mT, depending on the temperature of the Hall sensor. At 25°C, the typical operating point is 7.5mT. The release point mirrors the operating point, at 25°C, the typical release point is -7.5mT. For ease of use, $\pm 7.5\text{mT}$ will be used for the operating- and release points.

3.4.1 Intrinsic Properties

The to be chosen magnets must retain their magnetisation at very high temperatures, due to the twenty sterilisation processes of 134°C they will be exposed to. It is preferable that the magnets' Curie temperature and operating point lie above the 134°C, so they survive the full 20 reprocessing cycles as specified in the requirements in section 2. The Curie temperature is the maximum temperature before magnets irreversibly lose all permanent magnetic properties, while the operating point is the maximum temperature before magnets start irreversibly losing permanent magnetic properties, leaving their performance weaker than before the magnet was heated.

There are two contenders for main choice of magnets. The choice either falls to Neodymium magnets, known for their high magnetic strength and resistance to demagnetisation. However, they do not have the high temperature resistance of other magnet materials; nevertheless, they can be used in applications with maximum operating temperatures of 220°C[23]. The other choice is Samarium Cobalt magnets, known to be slightly less powerful than Neodymium magnets, however they are extremely resistant to demagnetisation at high temperatures, and are often used in the aerospace and medical sectors[24].

Samarium Cobalt magnets were chosen to ensure consistent performance during the sterilisation process, and because there were no Neodymium magnets available with a high enough operating temperature for the sterilisation process. According to the datasheet[25], the chosen magnets have an operating point of 250°C, far higher than the needed 134°C. This makes the magnets suitable for the operational environment of the ADEPTH, and a reasonable choice for the prototype.

3.4.2 Simulation

An important design choice is the strength of the magnets, they have to have a sufficiently high remanence to produce the necessary magnetic flux density to switch the Hall sensor on or off. Another important design choice is the amount of magnets in the rotating ring: too few and the user has to rotate too much to switch, the sensitivity is too low; too many and the switching

can happen too fast, the sensitivity of the switching is too high. An educated guess on the needed remanence and magnet quantity can be made and then tested experimentally, or the entire prototype setup can be simulated.

To simulate whether the Hall sensor will switch, the accumulated magnetic flux density of all present magnets can be calculated at the location of the Hall sensor. This can more easily be done by modeling the magnets as magnetic dipoles, and using their respective magnetic moments to calculate each magnets' impact on the magnetic flux density.

The magnetic flux density per magnetic dipole can be calculated using Equation 7:

$$\mathbf{B} = \frac{\mu_0}{4\pi} \left(\frac{3\mathbf{r}_{rel}(\mathbf{m} \cdot \mathbf{r}_{rel})}{r^5} - \frac{\mathbf{m}}{r^3} \right) \text{ [T]} \quad (7)$$

where μ_0 is the permeability of free space, \mathbf{r}_{rel} is the relative position vector from source to observation point, \mathbf{m} is the magnetic moment vector of a magnetic dipole, and r is the magnitude of the relative position vector.

The relative position vector \mathbf{r}_{rel} is calculated as follows:

$$\mathbf{r}_{rel} = \mathbf{r} - \mathbf{r}_0 \quad (8)$$

where \mathbf{r} is the position vector of the observed point, and \mathbf{r}_0 the position vector of the magnetic dipole.

The magnetic dipole moment can be calculated using Equation 9:

$$\mathbf{m} = M \cdot V \hat{\mathbf{u}} \text{ [Am}^2\text{]} \quad (9)$$

where M is the magnetisation field, V is the volume of the magnet, and $\hat{\mathbf{u}}$ is the unit vector indicating the direction of the magnetic dipole moment.

The magnetisation field is calculated as follows:

$$M = \frac{B_s}{\mu_0} \text{ [A/m]} \quad (10)$$

where B_s is the remanence, which is an intrinsic property of a magnet, and μ_0 is once again the permeability of free space.

The interacting magnetic fields between dipoles were simulated for a range of one through twelve dipoles using the code in Appendix B. Only the simulated plot for six dipoles is shown in Figure 10, as that is the amount of magnets chosen to be in the rotating rings of the prototypes; the figures for the other dipoles can be found in Appendix C. Figure 10 shows the hull of the ADEPTH as a black circle, the magnetic dipoles with their directions as blue arrows, the Hall sensor as a red dot, the magnetic field lines as green arrows, and a permanent magnet used to give a feeling of feedback as the ring is rotated as a red arrow. Due to time constraints, the permanent feedback magnet was not worked out further, and can be ignored.

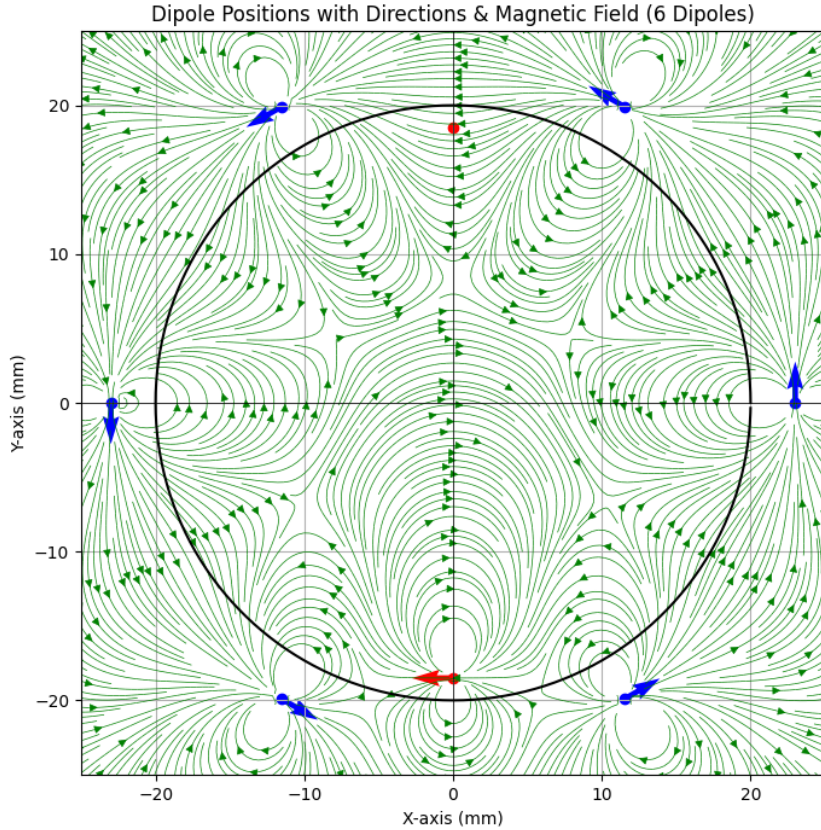


Figure 10: Simulated magnetic field with 6 dipoles. Black circle represents the ADEPTH hull. Blue arrows represent the magnetic dipoles. Red arrow represents the feedback magnet. Red dot represents the Hall sensor. Green arrows represent the magnetic field lines.

Figure 11 and Figure 12 show the magnetic flux density at the Hall sensor in the x- and y-planes as the magnets rotate 360° around the hull, respectively. As the chosen Hall sensor is sensitive to magnetic flux in the x-plane[21], the speed and direction output signals trigger between high and low when the magnetic flux density in the x-plane crosses the thresholds of $\pm 7.5\text{mT}$. This behaviour can be seen in Figure 11 as the red block wave. The plot also shows that the magnetic flux density ranges from approximately -20 to 55mT , indicating that the remanence of 900mT of the chosen magnet[25] is sufficient to trigger the Hall sensor.

A quick verification of the plots is beneficial to confirm whether the simulation results are accurate. The magnetic field lines in Figure 10 should travel from the north to the south poles of the magnetic dipoles, with the north poles at the tips of the arrows and the south poles at the dotted bases. The field lines extend from the north poles to their corresponding south poles as well as to the south poles of nearby dipoles. This behavior aligns with theoretical expectations, suggesting that the magnetic flux density calculations are most likely correct.

The magnetic flux density in the x-plane at the Hall sensor in Figure 11 should peak every $\frac{360}{6} = 60^\circ$, corresponding to a magnetic dipole being directly overhead and parallel to the Hall sensor. This maximizes the magnetic flux density in the x-plane while minimizing the density in the y-plane. As the dipoles rotate around the outer ring and approach the Hall sensor, the x-plane density should drop to zero when the magnet is almost overhead as the field lines only have a y-component, corresponding to a minimum in Figure 12. When the magnet reaches the parallel overhead position, the x-plane density peaks, corresponding to a maximum in Figure 11. As the magnet starts to move away, the density in the x-plane reaches zero, while the y-plane reaches a maximum in Figure 12. As the magnet continues to move away from the Hall sensor, the flux

density flowing from its south pole to the north pole of the following dipole passes through the Hall sensor, resulting in negative flux density. As the dipole moves further and further away from the Hall sensor, the flux densities in both planes should approach zero, as seen in the plots up to six dipoles in Appendix C. Finally, as a new dipole approaches, the flux density in the x-plane should go negative before returning to zero. Both Figure 11 and Figure 12 reflect these expectations, thus confirming the accuracy of the magnetic flux density calculations at the Hall sensor.

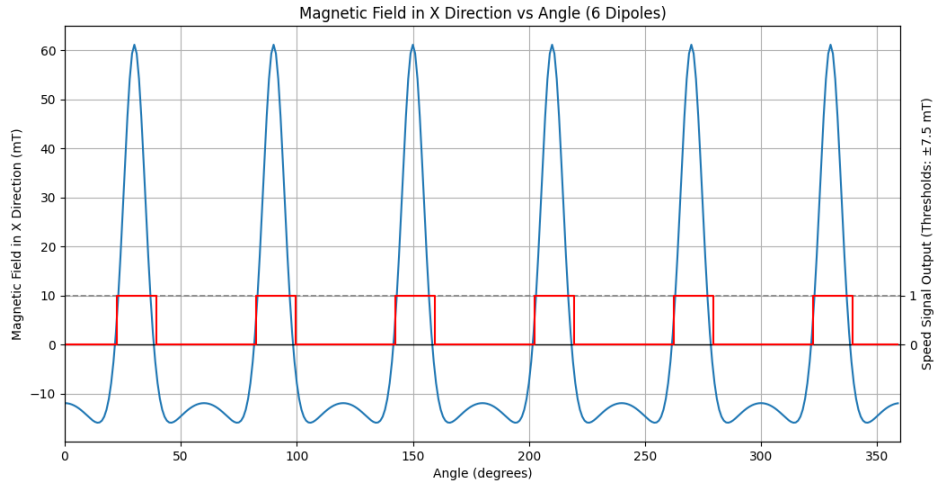


Figure 11: Simulated magnetic field along the x-plane of the Hall sensor for 6 dipoles versus angle. Blue waveform is the magnetic field density along the x-plane at the Hall sensor. Red waveform is the corresponding logic speed signal output of the Hall sensor, triggered at ± 7.5 mT.

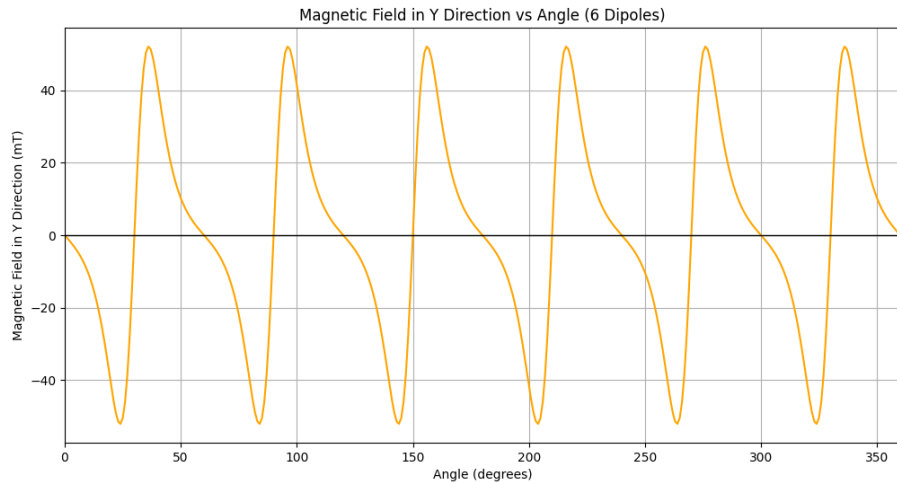


Figure 12: Simulated magnetic field along the y-plane of the Hall sensor for 6 dipoles versus angle.

Based on the simulations and the rotation sensitivity requirement, the number of magnets was narrowed down to six, seven, or eight. Experimentally, six magnets were found to be of sufficient efficiency, albeit barely. Meaning eight magnets would also be satisfactory, and it is likely dependent on user preference. Extensive user testing must be performed to determine the most comfortable option.

3.5 Prototype 3D Design

Now that it is clear which sensor and magnets will be used and how they work, it is time to consider how they can be implemented into the hull of the ADEPTH. To ensure that the workflow of the operating room is not disturbed, a natural and ergonomic solution must be developed. Additionally, it is crucial that all components remain safely within the watertight housing. The six magnets can be positioned on the outside during the sterilization process. Several initial designs have emerged from these considerations.

3.5.1 Rapid prototyping

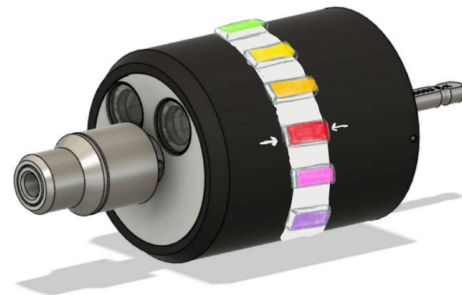
The first idea and design is based on a rotary switch where the pivot point is precisely in the center, see Figure 13a. However, this design is not feasible for implementation with the ADEPTH, as it has a shaft that would pass through the center of the rotary knob, making it impossible to turn the drill and to keep the hull watertight.

This quickly led to a new design where the mechanism rotates around the hull with the use of an outer ring. Inspiration was drawn from how such a mechanism works on a regular drill. This can be implemented in various ways. In Figure 13b a drawing of this first idea was made. Based on this drawing, a rapid prototype was made, which can be seen in Figure 13c.

To more effectively visualize the ideas and prototypes, time was invested in learning a 3D modeling program, Autodesk Fusion 360. By creating models in this program first, they could then be 3D printed. A result of the first model can be seen in Figure 13d.



(a) Rapid prototype design for rotary knob.



(b) Drawing of ring idea on ADEPTH.



(c) Rapid prototype design.



(d) First 3D printed design.

Figure 13: First designs for implementation on the ADEPTH.

The magnetic dipole moment \mathbf{m} is in the negative x-direction, so Equation 11 becomes:

$$B = \frac{\mu_0}{4\pi} \left(\frac{m}{r^3} \right) \text{ [T]} \quad (12)$$

Taking the position of the remanence of the magnet as r_0 , and the position of the Hall sensor as r_1 , Equation 12 can be written as two equations:

$$B_0 = \frac{\mu_0}{4\pi} \cdot \frac{m}{r_0^3} \quad (13)$$

$$B_1 = \frac{\mu_0}{4\pi} \cdot \frac{m}{r_1^3} \quad (14)$$

The magnetic moment m , μ_0 , and 4π stay the same value as the perpendicular distance between Hall sensor and magnet changes. With this information, the two equations can be equated to each other:

$$B_0 \cdot r_0^3 = \frac{\mu_0}{4\pi} \cdot m \quad (15)$$

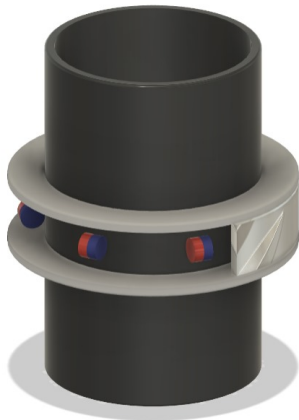
$$B_1 \cdot r_1^3 = \frac{\mu_0}{4\pi} \cdot m \quad (16)$$

Equating Equation 15 and Equation 16 leads to Equation 17, which is used to determine the maximum distance the magnets can be from the Hall sensor:

$$r_1 = \sqrt[3]{\frac{B_0 \cdot r_0^3}{B_1}} \quad (17)$$

$$r_1 = \sqrt[3]{\frac{900\text{mT} \cdot (1\text{mm})^3}{7.5\text{mT}}} = 4.93\text{mm} \quad (18)$$

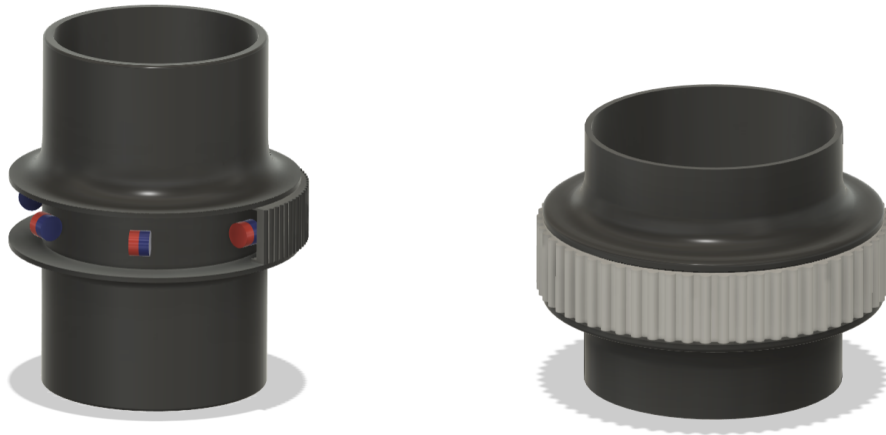
Equation 18 shows that the maximum thickness of the hulls can be at most 4.93mm before the Hall sensor is no longer triggered by the magnets.



(a) First 3D model with magnets and ring.



(b) Second 3D model where grip is added to the ring.



(c) Third 3D model with adjusted grip and smooth edges.

(d) 3D model with the dimensions of the ADEPTH.

Figure 15: Iterations of the 3D models for prototype designs.

The first 3D model can be observed in Figure 15a. After this initial design was 3D printed, it was possible to test and apply improvements. The second design, shown in Figure 15b, features grip on the ring, making it easier to turn. For the third design, seen in Figure 15c, the grip was further improved, and all sharp edges were smoothed out to make the design easier to clean and to give it a more streamlined appearance. Ultimately, all these improvements were combined in a design that follows the dimensions of the ADEPTH from Figure 14, which is shown in Figure 15d.

3.5.3 Final 3D design

The final model, as illustrated in Figure 16, includes a lid to conceal the electronics, leaving only the indication LEDs visible. To ensure the magnets remain securely in place without the need for adhesive, six small compartments matching the size of the magnets have been integrated into the ring. This design not only improves the overall aesthetics by hiding the internal components, but also enhances the functionality by providing a dedicated and secure housing for the magnets.

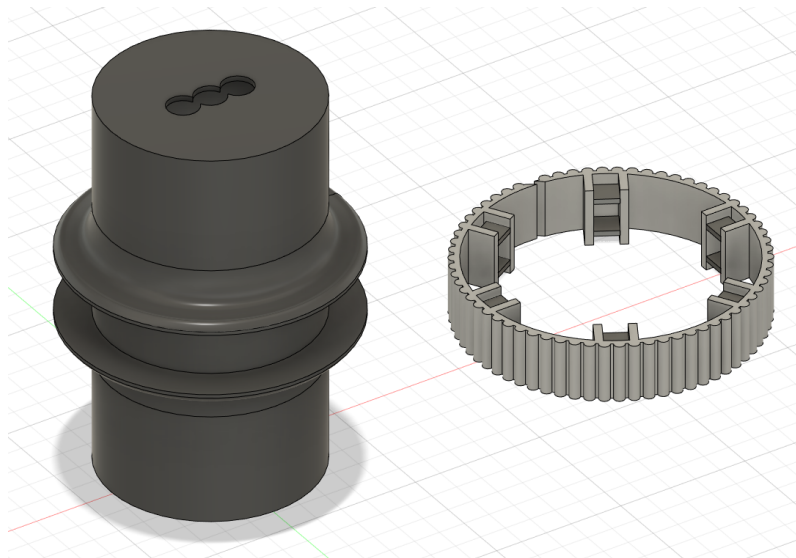


Figure 16: Final 3D model of the prototype.

3.6 Micro controller

To know whether the prototype works, three indication LEDs are integrated into the prototype to give visual feedback as to whether the Hall sensor correctly intercepts whether the ring rotates left or right. The Hall sensor alone cannot automatically control LEDs to behave in the desired manner; for this, a micro controller is required. Both an Arduino and Adafruit Feather[26] were used in this project. The first prototype was made with a breadboard and a programmable Arduino to read out the Hall sensor. The circuit for this prototype can be seen in Figure 17. The prototype build on the breadboard can be seen in Figure 18.

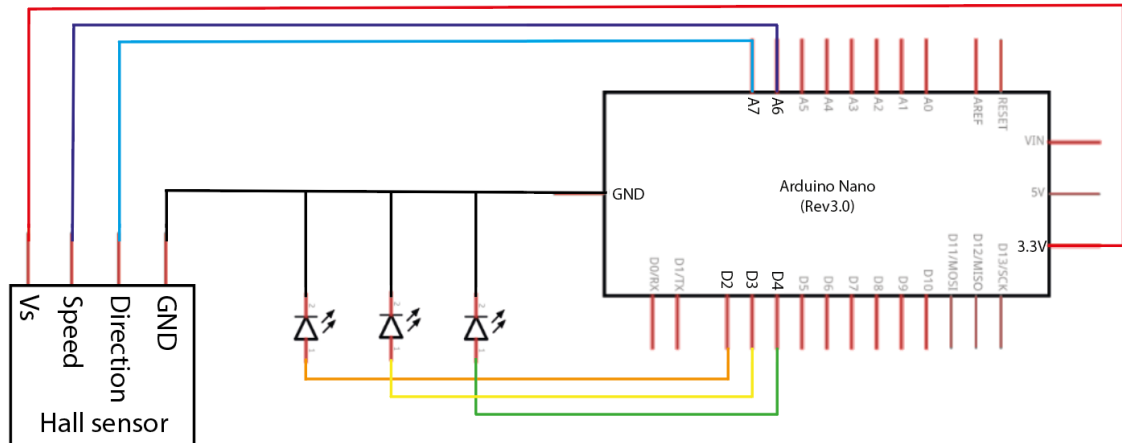


Figure 17: Circuit of the prototype with the Arduino.

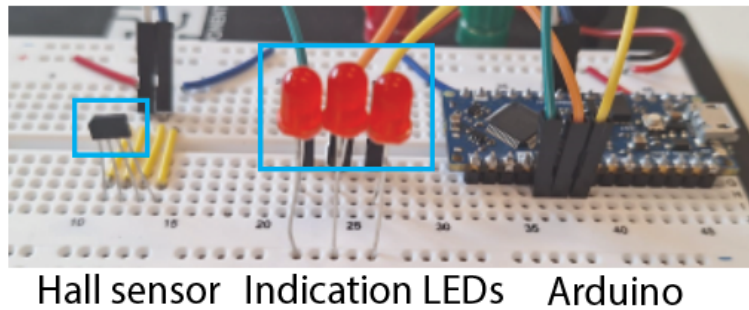


Figure 18: Prototype of the breadboard with Hall sensor.

The Arduino powers the Hall sensor, and also reads out the logical high or low data from the direction and speed pin. Both the direction and speed pins are connected to the Arduino with a pull-up input. Figure 19 shows how the Arduino receives input from the Hall sensor pins. In Figure 19a the switch is closed, so the Hall sensor pin will be connected to ground and result in a low (0V) signal at the Hall sensor. In Figure 19b the switch is open, and thus the Hall sensor pin is not connected to the ground. Consequently, no current will go through the resistor, and the pin outputs a high (3.3V) signal at the Hall sensor.

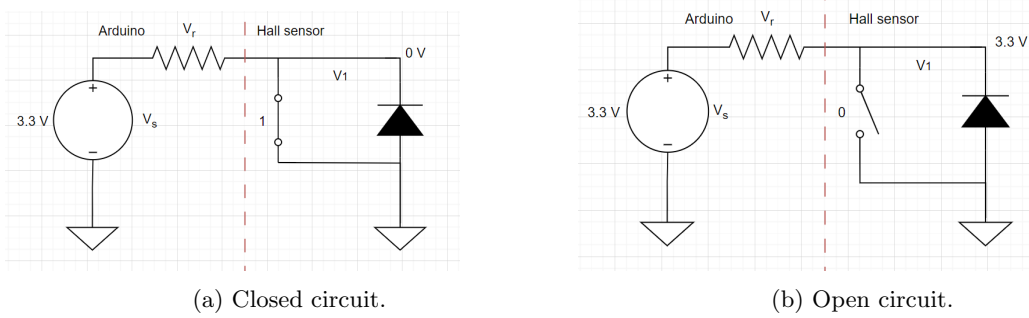


Figure 19: Pull-up electric circuit of the micro controller.

The voltage measurements were conducted between the Hall sensor output pins and the ground. However, the Arduino measures the voltage difference across the resistor, resulting in inverted inputs compared to the measurements taken at the Hall sensor side, as explained in subsection 3.3. Direct measurements over the resistor were not possible, because it is located inside the Arduino. Consequently, the Arduino registers a high input when the switch is closed and a low input when the switch is open. This inversion is crucial for the power calculations discussed in section 4, as the measured values are inverted from the original measurement location.

Now that the Arduino signals are clear, the waveform needs to be understood. Figure 20 shows the wave forms for the speed and direction signals. The direction signal is high when turned right, and low when turned left, relative to the Hall sensor. The direction signal only indicates the last observed direction of rotation to either the left or right, and does not pulse repeatedly when another magnet passes by. This is where the speed signal comes into play, however, the speed signal waveform is more complex. The signal is pulsed the opposite direction relative to the direction signal's value. When the magnets are turning right relative to the Hall sensor, the speed signal is pulled high and pulses low. When the magnets are turning left, the speed signal is pulled low and pulses high, as can be observed in Figure 20. Additionally, when there is a change of direction, the speed signal will follow the direction signal's waveform.

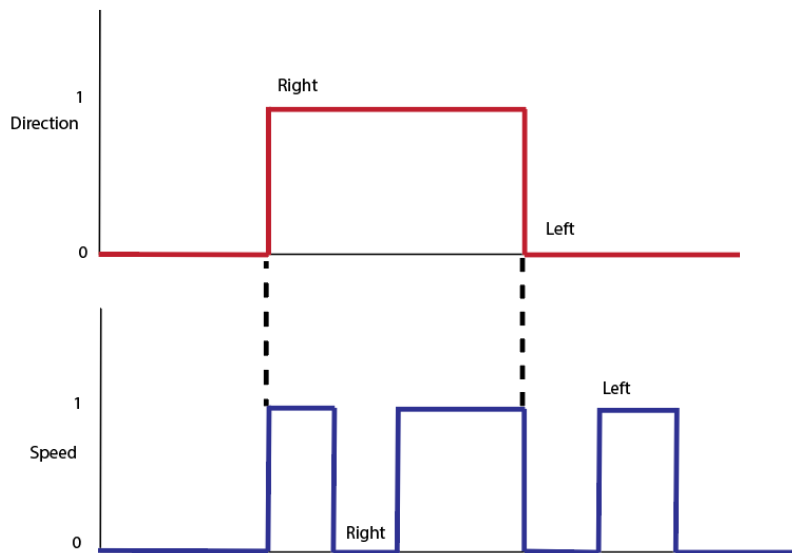


Figure 20: Waveform received at the micro controller.

3.7 Prototyping Board

Once the prototype on the breadboard was operational, a prototype could be made that could fit inside a 3D printed hull. The prototype was built on a prototyping board to minimise the amount of space it would take up. The 3D hull has six magnets on the inside of the rotating ring, as argued for in subsection 3.4. After soldering the wires and securing the magnets with a hot glue gun, the first prototype was ready for testing. Testing concluded that the magnet ring had enough feedback, and the prototype circuit board functioned as expected. These result can be found in section 4.

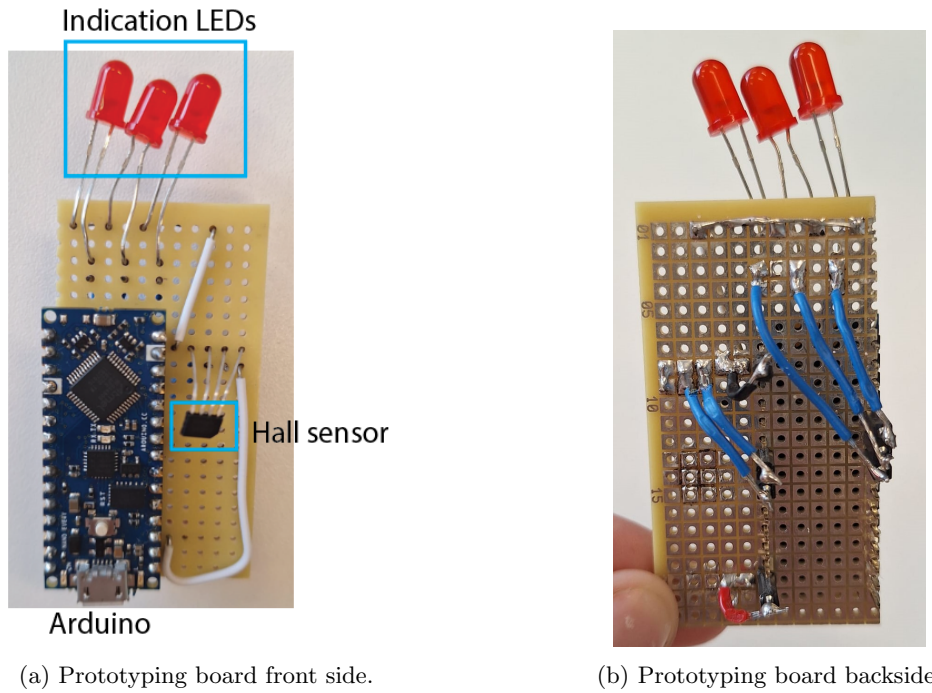


Figure 21: Prototyping board with Arduino.



Figure 22: First complete prototype and a close up of the magnetic ring.

3.8 Wireless communication

At some point, the prototype needs to function wireless, as depicted in Figure 23. The figure shows how the system would end up communicating with the already existing hardware. The wireless prototype would still have the hardware outside of the ADEPTH.

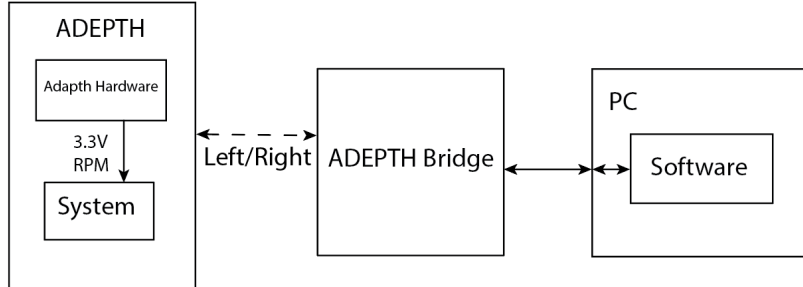


Figure 23: Communication block diagram for the wireless connection.

After verifying the functionality with the Arduino, the focus shifted to implementing wireless communication using the Feather board. The Feather board was initially tested on a breadboard, as shown in Figure 24, to evaluate the wireless communication capabilities and ensure compatibility with the existing Arduino code.

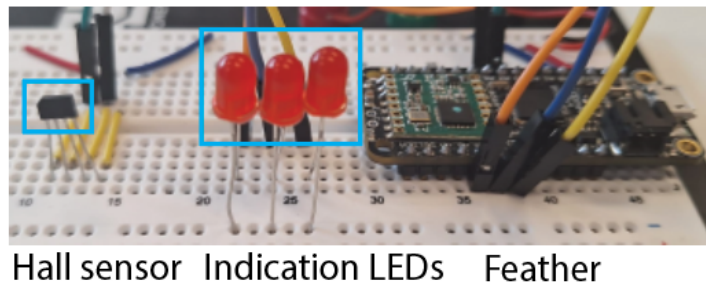


Figure 24: Prototype with Feather board.

In subsection D.2 & subsection D.3, the code for the send-Feather and receive-Feather can be found. The send-Feather sends 'right' or 'left' character strings, the receive-Feather then receives those strings and outputs them with a print statement. The send-Feather also has the code to decide when the 'left' & 'right' need to be sent, the inner workings for this are explained in subsection 3.9.

3.9 Code and FSM

After understanding how the signals work, code needs to be written to process those signals. In subsection D.1 & subsection D.2, the code for the Arduino & Feather can be found. The codes are mostly similar, the only difference is that the Arduino does not use wireless communication.

The code is based on edge detection: when the previous value of the pin is different from the current value, an action is taken. There are two parts to the code: edge detection, and a finite-state machine (FSM). Edge detection is done on the direction pin, and the FSM is implemented for the speed sensor. Figure 25 shows the waveforms and indicates when the code outputs a 'right' or 'left'. The code gives higher priority to the edge detection of the direction and thus will always trigger when the magnets turn a different direction. If the direction sensor changes to a '1' it will output 'right', if it changes to '0' it will output 'left'.

If that is not the case, the edge detection for the speed sensor takes place. However, because it is a pulse, there cannot be just edge detection. Following the speed waveform in Figure 25, it can be seen that the code starts in the *idle_start* state. It will wait until the previous signal and the current signal are no longer the same. When they have different values, the turn state is entered, where

the direction sensor is read out to determine which direction is turned to. Immediately afterward, the *idle_finish* state is entered, where it will idle until the previous signal and the current signal have different values again. This marks the end of one turn, and the speed signal has returned to its original value (the same value as the direction). Figure 26 shows the FSM on which the code in subsection D.1 & subsection D.2 is based.

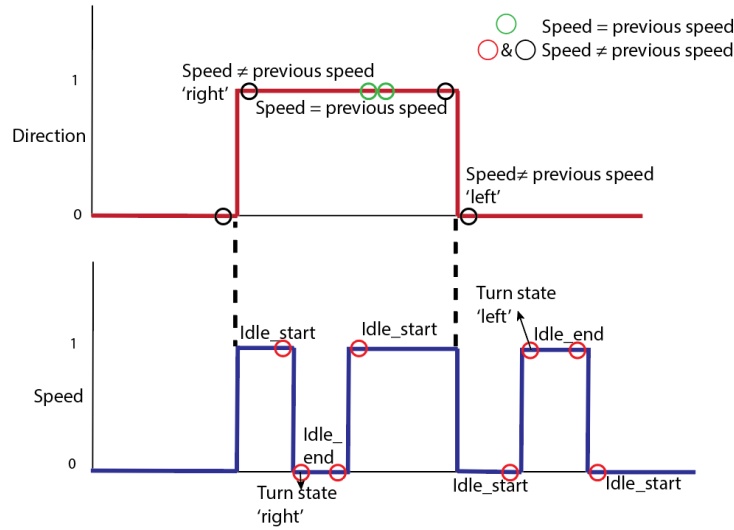


Figure 25: Waveform with states changes.

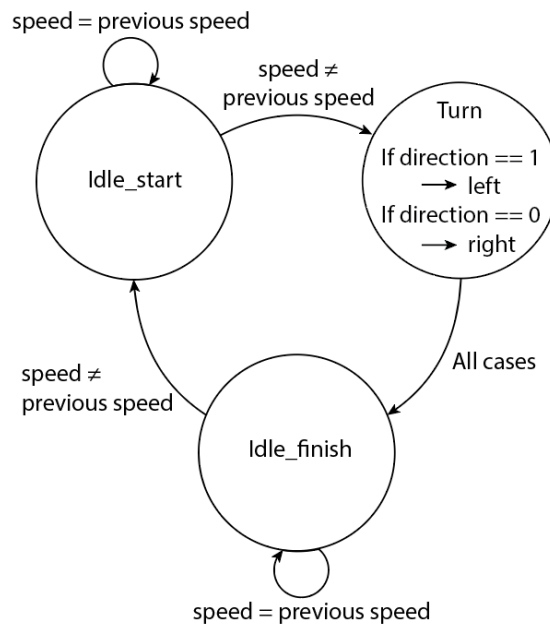


Figure 26: FSM.

In the code, there are also some features unrelated to determining the direction of the turn. These include the control of LEDs, button status, and wireless communication. The LEDs are designed to resemble the selection system on the computer screen; these three LEDs have been assigned integer pin numbers, and a variable 'i' will cycle through these LEDs using modulo 3. When the ring of magnets turns left, 'i' will decrease in value, and increase in value when the ring turns right.

The button's function is to mimic the condition during drilling, and no data from the Hall sensor needs to be read out. The last feature is wireless communication, it sends out a string of characters,

'left' or 'right', to another Feather board; this board connects to SLAM Orthopaedic's code, which controls the screw type selection method onscreen.

3.10 Selection mechanism

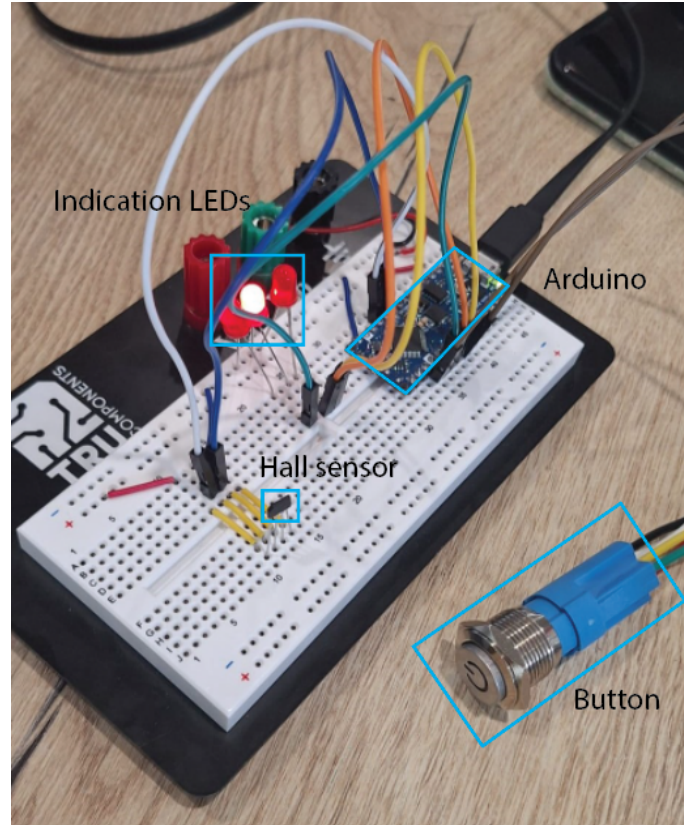


Figure 27: Prototype with button.

The final addition to the prototype is the selection mechanism. The chosen selection method, which felt most intuitive and least invasive for workflow, first involves cycling through the different screw types, and second to drill with the selected screw type. The implementation for the system would be that if the ADEPTH rotates faster than 100 RPM, which it calculates using two gyroscopes present in the ADEPTH, the screw type selected at that speed is the one used. In the prototype, the implementation is simulated by pressing a button that represents the RPM being faster than 100. In Figure 27, the prototype with the button implemented can be seen. The way the code works is explained in subsection 3.9.

4 Results

In this chapter, it will be examined whether the prototype meets the requirements specified in section 2. The focus will mostly be on the must haves from the technical requirement in subsection 2.5.

4.1 Power usage

In order to determine whether the prototype complies with the technical requirements, both the voltage and current needs to be measured. A set up was made in the Tellegen hall where these were measured at the same time, see Figure 28. The measurement was done with the Feather powering the Hall sensor, because the Feather is most representative of 'The System'. With the measured voltage and current, both the power and internal resistance could be calculated. Due to the difference between left and right signals, the Hall sensor does not have a continuous value. It was assumed that rotation would occur equally to the left and right. This assumption does not make a big difference in calculated power, as the supply voltage draws the most power and also remains the most stable between left and right.

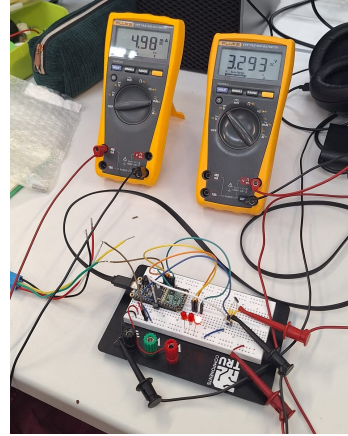


Figure 28: Test set up for the power usage measurements.

Input	Left to Right	Right to Left	Average Power	Internal resistance
Supply voltage pin (V)	3.293	3.293	16.43 mW (19)	
Supply voltage pin (mA)	4.97	5.01		
Direction pin (V)	0.019	3.290	0.0174 mW (20)	32.9 kΩ (21)
Direction pin (mA)	0.10	0.01		
Speed pin (V)	0.024	3.290	0.0177 mW	32.9 kΩ
Speed pin (mA)	0.10	0.01		
Total	5.17 mA	5.03 mA	16.61 mW	

Table 2: Power usage.

The average power drawn per pin:

$$P = \frac{3.293 \cdot 4.97 \cdot 10^{-3} + 3.293 \cdot 5.01 \cdot 10^{-3}}{2} = 16.43\text{mW} \quad (19)$$

$$P = \frac{0.019 \cdot 0.1 \cdot 10^{-3} + 3.290 \cdot 0.01 \cdot 10^{-3}}{2} = 0.0174\text{mW} \quad (20)$$

The internal resistance of the pull-up pin from the Arduino, which can not be altered, is calculated by using the current when the switch is closed (left -> right) and the voltage when the switch is open (right -> left). This approach is used to determine both the voltage difference across the resistor and the current through the resistor, which cannot be measured directly.

$$R = \frac{V}{I} = \frac{3.290}{0.1 \cdot 10^{-3}} = 32.9\text{k}\Omega \quad (21)$$

Table 2 shows that the prototype uses less than the absolute maximum of 12V, only 3.3V. This satisfies both the prototype and system requirements for the voltage usage. The prototype also only uses around 5.1mA continuous, and at most 5.17mA. This is far below the 62.5mA continuous

standby and 500mA pulse requirement. The system uses roughly 5.1 mAh, and this accounts for about 2% of the battery life.

The Hall sensor is 5.34mm in width, so the requirement of it fitting inside the diameter of the ADEPTH (38mm), is also satisfied. The 3D modeled hull diameter is 53mm, which is smaller than the absolute maximum diameter of 60mm. The Hall sensor and magnets are able to withstand 134°C and were chosen with that requirement in mind. This indicates that the prototype satisfies all technical requirements. All realised and unrealised requirements of the prototype can be observed in Table 3.

Requirement	Realized	Explanation
Uses less than 12V.	Yes.	Runs on 3.3V.
Shouldn't use more than 500mA, for a pulse of 15s.	Yes.	Peaks at 5.17mA.
Shouldn't use more than 62.5mA when on standby.	Yes.	Uses 5.1mA continuous.
Electronics smaller than diameter of 38mm.	Yes.	Hall sensor is 5.34mm.
Should not exceed total diameter of 60mm.	Yes.	The 3D modeled hull diameter is 53mm.
Hardware should be able to withstand 134°C.	Yes.	Magnets go up to 250°C & Hall sensor up to 195°C.
Uses no more than 25% of a battery of 250mAh.	Yes.	Uses 5.1mAh.
Prototype is watertight.	No.	Prototype hull contains holes for indication LEDs & to insert the electronics.
Selects correct screw during procedures.	Yes.	Can cycle through screw options & select correct one.
Controlled by surgeon / sterile assistant.	Yes.	Surgeon / assistant can control the prototype.
Intuitive to the user & ergonomic.	Yes.	Found to be intuitive (Appendix E).
Prototype is resistant to steam autoclave sterilisation.	No.	Material used for the 3D print will melt.
Provides input to the ADEPTH Software.	Yes.	Done through UART or 868MHz Data Transfer.

Table 3: Realised requirements for the prototype.

4.2 Demonstration

The prototype satisfies all the prototype requirements, but is yet to show that it actually works. Figure 29 shows that the prototype is able to selected the next screw type. These images are a part of a user test, which can be found in Appendix E. The test shows the steps taken to change the screw type with the prototype. Figure 29 also shows that the surgeons can choose a new screw type after completing the drilling. The surgeon selects the next screw type by rotating the ring to the desired screw type. The next screw type is the green locking screw. The orange rectangle in Figure 29b shows that the locking screw is selected instead of the cortical in Figure 29a.



(a) The cortical (yellow) screw type has been selected.



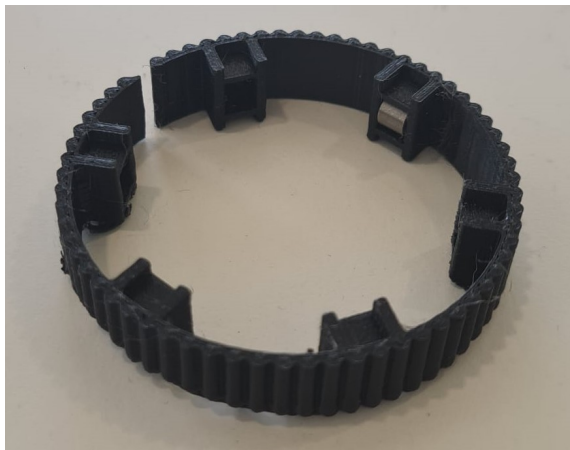
(b) The next screw type, locking (green), is selected by rotating the ring.

Figure 29: Demonstration of the selection method.

In Figure 30a, the final prototype can be seen, which was designed in subsection 3.5.3. This is the prototype that will be used in future user tests. After doing this test, it was clear that this solution works well and does not notably interrupt the work flow. The surgeons no longer have to use the touch screen, allowing them to maintain their focus on the procedure. This improvement streamlines the workflow, enabling the surgeons to continue their tasks seamlessly and efficiently without the use of a touch screen.



(a) The final prototype.



(b) The ring of the final prototype.

Figure 30: The final prototype.

5 Discussion of results

The results presented in the previous section show, after thorough examination, that the power usage of the Hall sensor incorporated into the ADEPTH is well within the specified technical requirements of subsection 2.5. The working prototype operates at 3.3V, far below the upper limit of 12V. Furthermore, the continuous current draw of roughly 5.1mA is far below the allowable 62.5mA in standby mode and the 500mA pulse requirement for fifteen seconds. The system uses roughly 5.1 mAh, and this accounts for about 2% of the battery life; which satisfies the less than 25% battery reduction requirement.

The magnet simulations from Figure 11 and Figure 12 show that the magnetic flux density at the Hall sensor is high enough to satisfy the thresholds necessary to trigger changes in the speed and direction signals. The flux density ranges from approximately -20mT to 55mT , which aligns well with the $\pm 7.5\text{mT}$ threshold of the Hall sensor. This also means that the 900mT remanence of the chosen magnets is sufficiently high.

Verification of the magnetic field simulations was useful to ensure the accuracy of the results. The observed behavior of the magnetic field lines and flux densities correspond with theoretical expectations, which substantiate the accuracy of the simulation models. The periodic maxima and minima in the x-plane flux density every 60 degrees, as well as the corresponding behavior in the y-plane, support the validity of the simulation approach: they both correspond with theoretical expectations.

The design of the ADEPTH system, including the positioning and number of magnets, was optimised for both functionality and user ergonomics. The decision to use six magnets in the rotating ring was based on a balance between limited supply, and the need to have some left over for further testing. However, extensive user testing must be performed for optimal balance between sensitivity and ease of assembly. This configuration ensures that the system can be operated intuitively without excessive rotation, which is essential for maintaining the natural workflow in an operating room. The 3D modeling and iterative prototyping process contributed to a design that is both practical and easy to use, as was verified during the user test in Appendix E.

In summary, the results indicate that the rotating ring prototype is a viable alternative for the touch screen to select the desired screw type. Its compliance with given technical requirements, combined with the successful verification of simulation results, demonstrates its potential for real-world application in an operating room.

6 Conclusion

This project aimed to enhance the ADEPTH system's interface for orthopedic surgeries by replacing the current touchscreen with a more suitable option for the operating room environment. Through research and evaluation, rotary encoding using a Hall effect sensor emerged as the most viable solution. This approach uses the intuitive nature of rotary switches, while meeting the requirements for sterility and seamless integration into the existing surgical workflow.

The Hall effect sensor operates by applying a fixed DC current across a semiconductor along one axis, and measuring the potential difference (Hall voltage) along another axis. This voltage is proportional to the axial component of the magnetic field that is perpendicular to both the current's axis and the sensing electrodes' axis. In this setup, the directions of the current, potential difference, and applied magnetic field align with the x-axis, y-axis, and z-axis, respectively.

Testing and prototyping demonstrated that the ADEPTH system with the integrated Hall sensor meets all technical requirements. The system operates at a low voltage of 3.3V (well below the 12V limit) and maintains a continuous current draw of approximately 5.1mA, significantly below the allowed 62.5mA in standby mode and the 500mA pulse requirement. The magnetic flux density simulations confirmed that the sensor operates outside the necessary thresholds of $\pm 7.5\text{mT}$, ensuring reliable speed and direction signal switching.

The iterative design process of the hull and ring, involving 3D modeling and prototyping, resulted in a practical and user-friendly solution. The final design features a rotating ring with six magnets, which strikes a balance between sensitivity and ease of use. This configuration allows for intuitive operation without excessive rotation, maintaining the natural workflow in the operating room.

In summary, the project successfully developed a rotary encoding interface using a Hall effect sensor for the existing ADEPTH system, enhancing its precision and efficiency in orthopaedic surgeries. This solution aligns with the requirements for sterility, intuitiveness, and integration into the existing workflow; demonstrating significant potential for real-world application. Future research should focus on optimising magnet size and exploring feedback mechanisms to further improve the system's performance and user experience.

7 Recommendation

After having completed this project with utmost delight, there are still some research questions left unanswered due to the short run time of this project. There was no time to test how much influence the rotation of the ADEPTH would have during drilling on the magnet ring, and whether that could cause an issue. If it does cause an issue, a different, incorrect screw could be selected, instead of the correct one.

Another unresolved question is what the minimum strength of a magnet should be, before they will be unable to trigger the Hall sensor. The smaller the magnet, the better; because they will have less inertia and also make the diameter of the ADEPTH smaller. After having spoken to professor Leon Abelmann, it was suggested to use neodymium magnets instead of Samarium Cobalt. Professor Leon shared that neodymium magnets could withstand 134°C , based on personally conducted experiments. The neodymium magnets are cheaper and usually smaller for the same amount of strength. Further research needs to be done to determine how much heat and sterilisation those neodymium magnets can handle.

Additionally, the possibility for a feedback mechanism to be implemented is mostly unanswered. There was not enough time to calculate the strength required for the feedback magnet, nor to determine how many were needed and in which configuration. The possibility of using an electromagnet for feedback was not looked into due to power constraints, nor the option of giving mechanical feedback. There was neither time to explore the use of a ferrous metal externally in the rotation ring, with only one permanent magnet behind the Hall sensor.

Furthermore, user testing must be preformed further to decide whether a ring with 6 or 8 magnets would be preferable. This needs to be executed, so a good balance between sensitivity and ease of assembly is found. During the user testing, the ergonomics of the ring could also be investigated.

References

- [1] “Va lcp™ ankle trauma system 2.7/3.5,” DePuy Synthes, Tech. Rep. [Online]. Available: https://synthes.hs.llnwd.net/o16/LLNWMB8/INT%20Mobile/Synthes%20International/Product%20Support%20Material/legacy_Synthes_PDF/164640.pdf.
- [2] *User manual adept system*, Mar. 2024.
- [3] SLAMORTHOPEDIC, Tech. Rep. [Online]. Available: <https://www.slamortho.com/adepth>.
- [4] J. Barker, *Interview with a plastic and orthopaedic surgeon*, Online Interview, Apr. 2024.
- [5] A. Gupta, “Operation room techniques for the surgeon,” *Prof BS Rana Memorial Oration*, p. 181,
- [6] W. A. Rutala and D. J. Weber, “Guideline for disinfection and sterilization in healthcare facilities, 2008. update: May 2019,” 2019.
- [7] M. Dion and W. Parker, “Steam sterilization principles,” *Pharmaceutical Engineering*, vol. 33, no. 6, Jan. 1, 2013. [Online]. Available: https://www.ispe.gr.jp/ISPE/07_public/pdf/201504_en.pdf.
- [8] B. de Hartog, *Interview with a orthopaedic surgeon and co-founder of slam orthopedic*, Online Interview, Apr. 2024.
- [9] “A world first: Reinier de graaf increases safety and efficiency with track and trace in the operating theatre.” (Feb. 2019), [Online]. Available: <https://www.tudelft.nl/en/2019/3me/february/a-world-first-reinier-de-graaf-increases-safety-and-efficiency-with-track-and-trace-in-the-operating-theatre>.
- [10] marManagement, “Rfid-technology for hospitals – add intelligence to your assets,” pp. 5–10. [Online]. Available: https://www.klsmartin.com/mediathek/91-350-16-02_marManagement-RFID.pdf.
- [11] E. Breshears and P. Bhargava, “Incorporation of Macropads Into Abdominal Imaging to Improve Radiologist Productivity and Efficiency,” *Current problems in diagnostic radiology*, Jul. 2023. DOI: 10.1067/j.cpradiol.2023.06.012. [Online]. Available: <https://www.sciencedirect.com/science/article/pii/S0363018823001007>.
- [12] M. Blaar, A. Janß, J. Dell’Anna, A. Höllig, K. Radermacher, and H. Clusmann, “Bottlenecks and needs in human-human and human-machine interaction – a view from and into the neurosurgical OR,” *Biomedizinische Technik*, vol. 61, no. 2, Jan. 2016. DOI: 10.1515/bmt-2015-0059. [Online]. Available: <https://doi.org/10.1515/bmt-2015-0059>.
- [13] D. Achacon Jr., D. Carlos, M. Puyaoan, *et al.*, “Realism: Real-time hand gesture interface for surgeons and medical experts,” 2010. [Online]. Available: https://www.researchgate.net/profile/Prospero_Naval/publication/268297823_REALISM_Real-Time_Hand_Gesture_Interface_for_Surgeons_and_Medical_Experts/links/54d470640cf2970e4e633443/REALISM-Real-Time-Hand-Gesture-Interface-for-Surgeons-and-Medical-Experts.pdf.
- [14] R. S. Popovic, *Hall Effect Devices* (Series in Sensors), Second Edition. Taylor & Francis, 2004, Available at Z-Library, ISBN: 9780750310151.
- [15] D. A. Neamen, *Semiconductor Physics and Devices: Basic Principles*, 4th. McGraw-Hill Education, 2020, Optional: Add any additional notes here, ISBN: 978-1259255579.
- [16] E. Tutorials, *Hall effect*, Accessed: 2024-06-10, 2024. [Online]. Available: <https://www.electronics-tutorials.ws/electromagnetism/hall-effect.html>.
- [17] A. MicroSystems, *Hall effect ic applications guide*, Accessed: 2024-06-10, 2024. [Online]. Available: <https://www.allegromicro.com/en/insights-and-innovations/technical-documents/hall-effect-sensor-ic-publications/hall-effect-ic-applications-guide>.
- [18] P. Horowitz and W. Hill, *The Art of Electronics*, 2nd. Cambridge University Press, 1989, ISBN: 978-0521370950.
- [19] E. Tutorials, *Open collector outputs*, Accessed: 2024-06-11, 2024. [Online]. Available: <https://www.electronics-tutorials.ws/transistor/open-collector-outputs.html>.

- [20] Y. Bellavance, *Own work*, <https://commons.wikimedia.org/w/index.php?curid=16834358>, CC BY-SA 3.0, 2024.
- [21] Infineon Technologies AG, *Tle4966l high precision hall-effect switch with direction detection*, V 2.0, <https://4donline.ihs.com/images/VipMasterIC/IC/INFN/INFNS13136/INFNS13136-1.pdf>, Feb. 2009. [Online]. Available: <https://4donline.ihs.com/images/VipMasterIC/IC/INFN/INFNS13136/INFNS13136-1.pdf>.
- [22] S. Solutions, *Chopper stabilization and gear tooth sensors*, Accessed: 2024-06-11, 2024. [Online]. Available: <https://sensorso.com/resources/chopper-stabilization-and-gear-tooth-sensors.html>.
- [23] A. LLC, *Magnetic materials*, Accessed: 2024-06-12, 2024. [Online]. Available: <https://allianceorg.com/magnetic-materials/>.
- [24] A. LLC, *Samarium cobalt magnets*, Accessed: 2024-06-12, 2024. [Online]. Available: <https://allianceorg.com/magnetic-materials/samarium-cobalt-magnets/>.
- [25] Infineon Technologies AG, *Tle4966l high precision hall-effect switch with direction detection*, V 2.0, <https://www.farnell.com/datasheets/91199.pdf>, Feb. 2009. [Online]. Available: <https://www.farnell.com/datasheets/91199.pdf>.
- [26] *Adafruit feather 32u4 with lora radio module*, RFM9x, Adafruit, Jun. 2024. [Online]. Available: <https://cdn-learn.adafruit.com/downloads/pdf/adafruit-feather-32u4-radio-with-lora-radio-module.pdf>.

A Surgeon Interviews

A.1 Interview John Barker

On the 23rd of April, an interview was held with John Barker who is a plastic (soft tissue) and orthopaedic (hard tissue) surgeon active in both clinical and research [4]. The interview started with an explanation of the project, what the product from SLAM is measuring, and what needs to be changed about it. During this interview, questions were asked to give more insight into how the OR (Operation Room) is operated and the rules. To make this conversation readable, some paraphrasing was used.

Q: Do you know before surgery which screws and plates you get, and do you get different lengths?

A: Before surgery they know the size of the screws they want to use from scans from x-rays, MRI, and CT scans. From those scans, they choose 3 to 4 sizes of screws they want to take into the OR. They don't know the dimensions of the plates exactly. During surgery, they select the screw that would fit, and if it's a bit too long they take it out and pick a different screw. For each surgery and situation, they pick which ones they need to use; so every surgery has a different set of screws.

Q: How many people are in the OR?

A: In an orthopaedic room there are 3 up to 10 people. The amount of people scrubbed in is a smaller number, somewhere between 2 and 5 people are sterile. The people in the OR who would be handling the touch screen would probably be around 4.

Q: Who would preferably select the screw type on the screen?

A: Preferably the surgeon if they have the freedom to do so. If you imagine building a house and having to ask someone else to do an action it's better to do it yourself.

Q: Which non-technical limitations should we take into account?

A: The surgeons are not prone to change anything in the OR or the way they want to do things. So the solution has to come with very little change in the OR. The surgeon already has to deal with a lot of information so nothing too overwhelming with data. The solution also needs to take into account that the errors due to mobility don't increase.

Q: What are some OR specific limitations for orthopaedic surgery?

A: In orthopaedics, unlike urology, is infection a big risk and lots is done to prevent infections. This means that the surgeon is double-gloved and in a kind of space suit to prevent any germs from getting near the bone. The dexterity of the surgeon is significantly lower and the buttons on the device should be big and fairly easily accessible. The device should also have a rough/textured and grippy surface, because during the operation there will be blood on the gloves. They can clean their hands during the surgery with gauze or a cloth, but it is still something to keep in mind.

Q: Regarding the robustness of the tools, what happens if it fails? is there a backup system?

A: The surgeons are like carpenters, they will find solutions to all problems. They are very versatile and resourceful, they will figure it out and make it work. Failure of a device is not a total emergency, but it is if the heart stops.

The interview ended with John asking us whether or not we wanted to see how such an operation unfolded.

A.2 Interview Bas de Hartog

On the 26th of April, an interview was held with Bas de Hartog [8]. He is an orthopaedic surgeon and co-founder of Slam Orthopedic. Slam Orthopedic was there to support us. To make this conversation readable some paraphrasing was used.

Q: How is communication managed inside the operating room, and how aware is the surrounding assistant of the situation, or are they busy with other tasks?

A: In a typical operation, there are three sterile team members, including two assistants and a surgeon. The operating room also has one surrounding assistant. The surrounding assistant's role is relatively minimal if the procedure is proceeding smoothly. Their main responsibility is to pass items like plates and screws from the non-sterile area to the sterile area upon the surgeon's request.

Q: Is there a different guide for every screw?

A: Whether a different guide is needed for each screw depends on the drill size, as the drill determines the guide.

Q: How are instruments passed by the sterile assistant?

A: The method of passing instruments varies; there is no universal technique. Each situation may dictate a different approach.

Q: Who might need to interact with electrical devices during a procedure?

A: The circulating assistant might not always be fully aware of the ongoing situation and could theoretically be replaced by a robot. In contrast, the sterile assistant is highly attuned to each step of the procedure, often anticipating the surgeon's needs and preparing for each step in advance without needing to be asked.

Q: Is the diagram in correct?

A: Yes, that's about right.

Q: What do you think about having a rotating disk on the ADEPTH?

A: It seems like a practical idea; it could streamline the workflow. The assistant could adjust the settings as needed, allowing me, as the surgeon, to focus solely on the procedure without concerns about adjusting the equipment.

Q: What would be the impact of using RFID tags in drill guides, implying the use of different guides for various types?

A: Incorporating RFID tags in drill guides could be a beneficial solution. However, if the RFID tags require close proximity to function, or if they must be attached to the guides around the drill, this could pose a limitation.

Q: Do you, as a surgeon, choose the screw when you need it?

A: Not every plate is compatible with all types of screws, the plate determines which can be used. I communicate what I'm doing, and the circulating assistant needs an active request to fetch the correct screw. Typically, we start with two cortical screws, followed by locking or variable angle locking screws.

Q: You already know the type of screw you're going to use, right?

A: Yes, knowing the correct type of screw in advance helps reduce waste. If we retrieve the wrong length or type of screw, it cannot be used and must be discarded.

Q: What if there was an external device that could communicate with the bridge, something like a numpad?

A: Integrating something on the ADEPTH itself would be more beneficial. Our trauma drill already has two settings, showing it can interact with buttons on the drill, so adapting it into the workflow could be effectively managed.

Q: What do you think of foot pedals?

A: Foot pedals are not commonly used and require a period of adjustment. They aren't inherently bad, but there are certainly more user-friendly options available. They likely wouldn't be the best solution for streamlining our workflow.

Q: What if an RFID tag needs to tap the ADEPTH?

A: It would be better if tapping isn't necessary, but rather just detecting within a certain range.

Q Bas: What if you display every type of screw on the screen?

A Slam: That could be overwhelming, considering three types of screws and two thicknesses, that's six variations. We believe displaying all these options might increase the likelihood of errors.

Q Bas: What about colour detection or QR code?

A Slam: Color detection can be unreliable because the guide might get dirty, altering how colours are perceived. QR codes require a high scan rate; currently, the ADEPTH handles 6 readings per cycle.

Bas: Sometimes we only have one hand free, and we need to manage the drill with that hand. Please take this into consideration.

Q: What about using a small remote controller?

A: A remote controller is a separate device, similar to a numpad. It could work, but a more elegant solution might be the rotary encoder. Every new solution requires some adjustment, so any option could be effective if designed properly. A straightforward, Apple-like solution would be ideal. However, simplicity is key.

B Python code for magnet simulation

```
import numpy as np
import matplotlib.pyplot as plt
import sys
import math
from scipy.interpolate import griddata

np.set_printoptions(threshold=sys.maxsize)

# Circle in mm
radius_sphere = 20 * 10**-3
radius_magnets = 23 * 10**-3
radius_hall_sensor = (radius_magnets - 4.5*10**-3)

# Constants
mu_0 = 4 * math.pi * 10 ** -7 # Vacuum permeability (Tm/A)
B_s = 925 * 10 ** -3 # Saturation flux density in Tesla (T)
radius_magnet = 2.5 * 10 ** -3 # Magnet radius in meters (m)
height = 4 * 10 ** -3 # Magnet height in meters (m)

# Function to get x and y coordinates of a circle
def get_x_y_coordinates(circles):
    xc, yc, r = circles
    theta = np.radians(np.arange(360)) # angles from 0 to 359 degrees in radians
    x = xc + r * np.cos(theta) # Calculate x coordinates
    y = yc + r * np.sin(theta) # Calculate y coordinates
    return x, y

# Function to get coordinates of dipoles evenly spaced around a circle
def dipole_coordinates(dipoles_number, circles):
    xc, yc, r = circles
    theta = np.radians(np.linspace(0, 360, dipoles_number, endpoint=False))
    x = xc + r * np.cos(theta) # Calculate x coordinates
    y = yc + r * np.sin(theta) # Calculate y coordinates
    return x, y

# Function to get coordinates of the hall sensor at a specific angle
def hall_sensor_coordinates(circles):
    xc, yc, r = circles
    theta = np.radians(90) # Hall sensor position at 90 degrees
    x = xc + r * np.cos(theta) # Calculate x coordinate
    y = yc + r * np.sin(theta) # Calculate y coordinate
    return x, y

# Function to get coordinates of a permanent magnet at a specific angle
def permanent_magnet_coordinates(circles):
    xc, yc, r = circles
    theta = np.radians(-90) # Permanent magnet position at -90 degrees
    x = xc + r * np.cos(theta) # Calculate x coordinate
    y = yc + r * np.sin(theta) # Calculate y coordinate
    return x, y
```

```

# Function to calculate magnetic flux density B at points r due to dipole
moments m at r0
def magnetic_flux_density(r, m, r0):
    r_relative = r - r0 # Relative position vector from source to field point
    r_magnitude = np.linalg.norm(r_relative, axis=1, keepdims=True) # Magnitude
    of r_relative
    r_magnitude[r_magnitude == 0] = np.inf # Avoid division by zero
    term1 = (3 * np.sum(m * r_relative, axis=1, keepdims=True) * r_relative) /
    r_magnitude ** 5
    term2 = m / r_magnitude ** 3
    B = (mu_0 / (4 * np.pi)) * (term1 - term2) # Calculate magnetic flux density
    return B

# Grid size and number of points for higher resolution
grid_size = 30
num_points = (grid_size * 4 + 1)

# Define range for x and y coordinates
x_range = np.linspace(-grid_size * 10 ** -3, grid_size * 10 ** -3, num_points)
y_range = np.linspace(-grid_size * 10 ** -3, grid_size * 10 ** -3, num_points)

# Create grid of coordinates
x_coords, y_coords = np.meshgrid(x_range, y_range, indexing='xy')
coordinates = np.dstack((x_coords, y_coords)).reshape(-1, 2)

# Define the circle parameters
circle_sphere = [0, 0, radius_sphere]
circle_magnets = [0, 0, radius_magnets]
circle_hall_sensor = [0, 0, radius_hall_sensor]

# Get the array of x and y coordinates for the circles
x_coords_circle, y_coords_circle = get_x_y_coordinates(circle_sphere)
x_coordinates_hall, y_coordinates_hall =
    hall_sensor_coordinates(circle_hall_sensor)
x_coordinates_magnet, y_coordinates_magnet =
    permanent_magnet_coordinates(circle_hall_sensor)

# Calculate magnetic moment
magnetization_field = B_s / mu_0 # Calculate magnetization field
volume = math.pi * radius_magnet ** 2 * height # Calculate volume of the magnet
magnetic_moment = magnetization_field * volume # Calculate magnetic moment

for dipole_number in range(1, 13):
    # Get dipole coordinates
    x_coords_dipoles, y_coords_dipoles = dipole_coordinates(dipole_number,
        circle_magnets)

    # Calculate dipole moments for each magnet
    dipole_moments = np.array([
        magnetic_moment * np.array([-y, x]) / np.linalg.norm([x, y])
        for x, y in zip(x_coords_dipoles, y_coords_dipoles)
    ])

    # Permanent Magnet Moment
    perm_magnet_moment = np.array([
        magnetic_moment * np.array([y_coordinates_magnet, x_coordinates_magnet])
        / np.linalg.norm(

```

```

        [x_coordinates_magnet, y_coordinates_magnet])
    ])

# Combine dipole moments and permanent magnet moment
dipole_moments = np.append(dipole_moments, perm_magnet_moment, axis=0)

# Compute the B field at all grid points
r0 = np.vstack(
    (np.column_stack((x_coords_dipoles, y_coords_dipoles)),
     [x_coordinates_magnet, y_coordinates_magnet]))

# Initialize the B_field array
B_field = np.zeros((coordinates.shape[0], 2))

# Vectorized computation of magnetic flux density
for i in range(r0.shape[0]):
    B_field += magnetic_flux_density(coordinates, dipole_moments[i], r0[i])

# Reshape B_field to match the grid shape
B_field = B_field.reshape(num_points, num_points, 2)
B_magnitude = np.linalg.norm(B_field, axis=2) # Calculate the magnitude of
the B field

# Interpolate magnetic field at the Hall sensor coordinates
hall_sensor_point = np.array([[x_coordinates_hall, y_coordinates_hall]])

# Convert coordinates to millimeters
x_coords_mm = x_coords * 1000
y_coords_mm = y_coords * 1000
x_coords_circle_mm = x_coords_circle * 1000
y_coords_circle_mm = y_coords_circle * 1000
x_coords_dipoles_mm = x_coords_dipoles * 1000
y_coords_dipoles_mm = y_coords_dipoles * 1000
x_coordinates_hall_mm = x_coordinates_hall * 1000
y_coordinates_hall_mm = y_coordinates_hall * 1000
x_coordinates_magnet_mm = x_coordinates_magnet * 1000
y_coordinates_magnet_mm = y_coordinates_magnet * 1000

# Plotting the magnetic field and dipole positions
plt.figure(figsize=(8, 8))
plt.streamplot(x_coords_mm, y_coords_mm, B_field[:, :, 0], B_field[:, :, 1],
    color='green', linewidth=0.5, density=5.0)
plt.plot(x_coords_circle_mm, y_coords_circle_mm, color='black', label='Outer
Shell')
plt.scatter(x_coords_dipoles_mm, y_coords_dipoles_mm, color='blue')
plt.scatter(x_coordinates_hall_mm, y_coordinates_hall_mm, color='red',
    label='Hall Sensor')
plt.scatter(x_coordinates_magnet_mm, y_coordinates_magnet_mm, color='red',
    label='Permanent Magnet')

# Plot quivers for dipole moments and permanent magnet moment
for x, y, dm in zip(x_coords_dipoles_mm, y_coords_dipoles_mm,
    dipole_moments):
    plt.quiver(x, y, dm[0], dm[1], color='blue', angles='xy')

plt.quiver(x_coordinates_magnet_mm, y_coordinates_magnet_mm,
    perm_magnet_moment[0, 0], perm_magnet_moment[0, 1],
    color='red', angles='xy')

```

```

plt.axhline(0, color='black', linewidth=0.5)
plt.axvline(0, color='black', linewidth=0.5)
plt.gca().set_aspect('equal', adjustable='box')
plt.xlim(-25, 25)
plt.ylim(-25, 25)
plt.xlabel('X-axis (mm)')
plt.ylabel('Y-axis (mm)')
if dipole_number == 1:
    plt.title(f'Dipole Positions with Directions & Magnetic Field
              ({dipole_number} Dipole)')
else:
    plt.title(f'Dipole Positions with Directions & Magnetic Field
              ({dipole_number} Dipoles)')
plt.grid(True)
plt.savefig(f'Magnetic_Field_Dipoles_{dipole_number}.png')
plt.close()
# plt.show()

# Initialize arrays to store the magnetic field at the hall sensor for each
# degree
Bx_at_hall_all = []
By_at_hall_all = []

# Number of unique positions to compute (360 / dipole_number)
unique_positions = 360 // dipole_number
remainder_positions = 360 % dipole_number

# Loop through the unique positions
for degree in range(unique_positions):
    theta = np.radians(degree)
    rotation_matrix = np.array([
        [np.cos(theta), -np.sin(theta)],
        [np.sin(theta), np.cos(theta)]
    ])

    # Rotate the dipole coordinates
    rotated_dipoles = np.dot(np.column_stack((x_coords_dipoles,
                                              y_coords_dipoles)), rotation_matrix.T)
    x_coords_dipoles_rotated = rotated_dipoles[:, 0]
    y_coords_dipoles_rotated = rotated_dipoles[:, 1]

#
    # Recompute dipole moments after rotation
    dipole_moments_rotated = np.array([
        magnetic_moment * np.array([-y, x]) / np.linalg.norm([x, y])
        for x, y in zip(x_coords_dipoles_rotated, y_coords_dipoles_rotated)
    ])

    # Combine the rotated dipoles and permanent magnet
    dipole_moments_combined = np.append(dipole_moments_rotated,
                                         perm_magnet_moment, axis=0)

    # Recompute the B field at all grid points
    r0_rotated = np.vstack((rotated_dipoles, [x_coordinates_magnet,
                                              y_coordinates_magnet]))
    B_field_rotated = np.zeros((coordinates.shape[0], 2))

    for i in range(r0_rotated.shape[0]):

```

```

        B_field_rotated += magnetic_flux_density(coordinates,
            dipole_moments_combined[i], r0_rotated[i])

B_field_rotated = B_field_rotated.reshape(num_points, num_points, 2)

# Interpolate magnetic field at the Hall sensor coordinates
Bx_at_hall_rotated = \
griddata(coordinates, B_field_rotated[:, :, 0].flatten(),
    hall_sensor_point, method='linear')[0]
By_at_hall_rotated = \
griddata(coordinates, B_field_rotated[:, :, 1].flatten(),
    hall_sensor_point, method='linear')[0]

# Save the results
Bx_at_hall_all.append(Bx_at_hall_rotated)
By_at_hall_all.append(By_at_hall_rotated)

# Repeat the unique results for the full 360 degrees
Bx_at_hall_all = np.tile(Bx_at_hall_all, dipole_number)
By_at_hall_all = np.tile(By_at_hall_all, dipole_number)

# Add remainder positions to cover the full 360 degrees
for _ in range(remainder_positions):
    Bx_at_hall_all = np.append(Bx_at_hall_all, Bx_at_hall_all[0])
    By_at_hall_all = np.append(By_at_hall_all, By_at_hall_all[0])
#
# Convert results to numpy arrays for easy manipulation
Bx_at_hall_all = np.array(Bx_at_hall_all)
By_at_hall_all = np.array(By_at_hall_all)
#
# Convert magnetic field results to millitesla (mT)
Bx_at_hall_all_mT = Bx_at_hall_all * 1000 # Convert to millitesla
By_at_hall_all_mT = By_at_hall_all * 1000 # Convert to millitesla

# Create an array for the angles
angles = np.arange(360)

# Generate a binary array for the block wave plot
block_wave = np.zeros_like(Bx_at_hall_all_mT)

# Initialize the state
state = 0

for i in range(1, len(Bx_at_hall_all_mT)):
    if Bx_at_hall_all_mT[i] > 7.5 and state == 0:
        state = 1
    elif Bx_at_hall_all_mT[i] < -7.5 and state == 1:
        state = 0
    block_wave[i] = state
#
# Plot the magnetic field in the x direction versus the angle
fig, ax1 = plt.subplots(figsize=(12, 6))
#
# Primary y-axis plot
ax1.plot(angles, Bx_at_hall_all_mT, label='Bx at Hall Sensor')
ax1.axhline(10, color='gray', linestyle='--', linewidth=1.2)
ax1.axhline(0, color='black', linewidth=1)

```

```

ax1.set_xlim(0, 360)
ax1.set_xlabel('Angle (degrees)')
ax1.set_ylabel('Magnetic Field in X Direction (mT)')
if dipole_number == 1:
    ax1.set_title(f'Magnetic Field in X Direction vs Angle ({dipole_number}
        Dipole)')
else:
    ax1.set_title(f'Magnetic Field in X Direction vs Angle ({dipole_number}
        Dipoles)')
ax1.grid(True)
# #
# Secondary y-axis for the block wave
ax2 = ax1.twinx()
ax2.step(angles, block_wave * 10, label='Block Wave (Thresholds: 7.5 mT)',
    where='mid', color='red', alpha=1)
ax2.set_ylabel('Speed Signal Output (Thresholds: 7.5 mT)')
ax2.set_yticks([0, 10])
ax2.set_yticklabels(['0', '1'])
ax2.set_ylim(ax1.get_ylim())
plt.savefig(f'Magnetic_field_x_{dipole_number}.png')
plt.close()
# plt.show()

# Plot the magnetic field in the y direction versus the angle
plt.figure(figsize=(12, 6))
plt.plot(angles, By_at_hall_all_mT, label='By at Hall Sensor',
    color='orange')
plt.xlim(0, 360)
plt.xlabel('Angle (degrees)')
plt.ylabel('Magnetic Field in Y Direction (mT)')
if dipole_number == 1:
    plt.title(f'Magnetic Field in Y Direction vs Angle ({dipole_number}
        Dipole)')
else:
    plt.title(f'Magnetic Field in Y Direction vs Angle ({dipole_number}
        Dipoles)')
plt.axhline(0, color='black', linewidth=1)
plt.grid(True)
plt.savefig(f'Magnetic_field_y_{dipole_number}.png')
plt.close()
# plt.show()

```

C Magnet Simulations

The magnetic flux density is simulated at the Hall sensor in the x- and y-plane. The magnetic field lines are also simulated for one through twelve dipoles, and their magnetic interactions between each other, and their interaction with the feedback magnet. The dipoles are the blue arrows, the feedback magnet is the red arrow, and the Hall sensor is the red dot. The black circle is the hull of the ADEPTH.

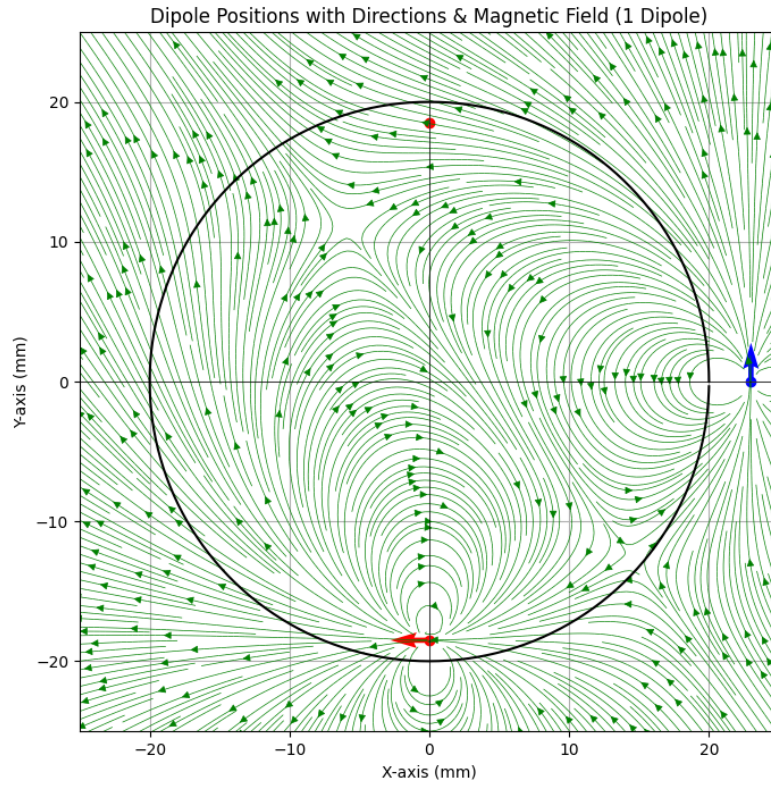


Figure 31: Simulated magnetic field with 1 dipole.

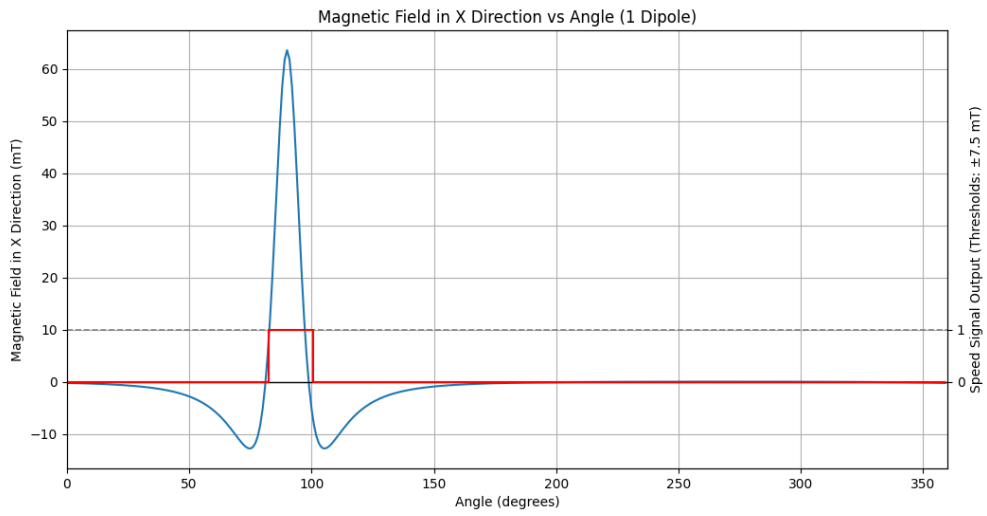


Figure 32: Simulated magnetic field along the x-plane of the Hall sensor for 1 dipole versus angle.

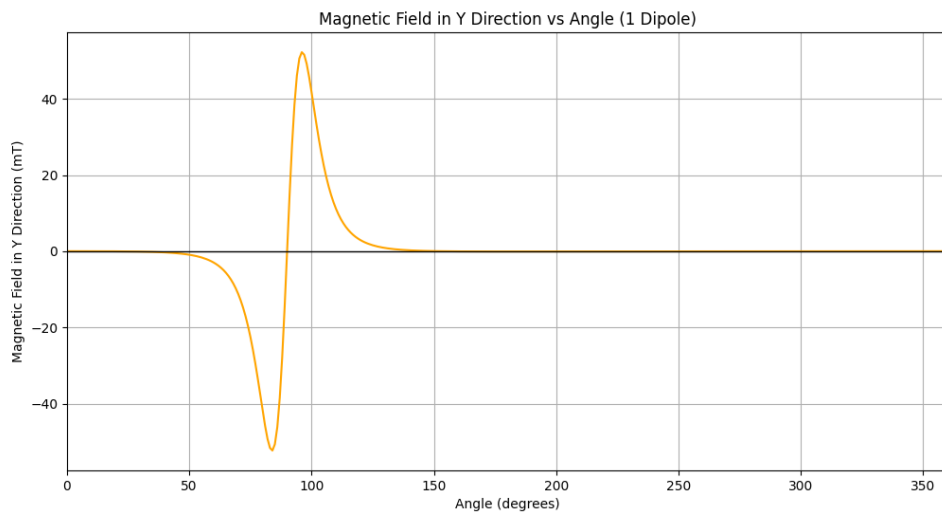


Figure 33: Simulated magnetic field along the y-plane of the Hall sensor for 1 dipole versus angle.

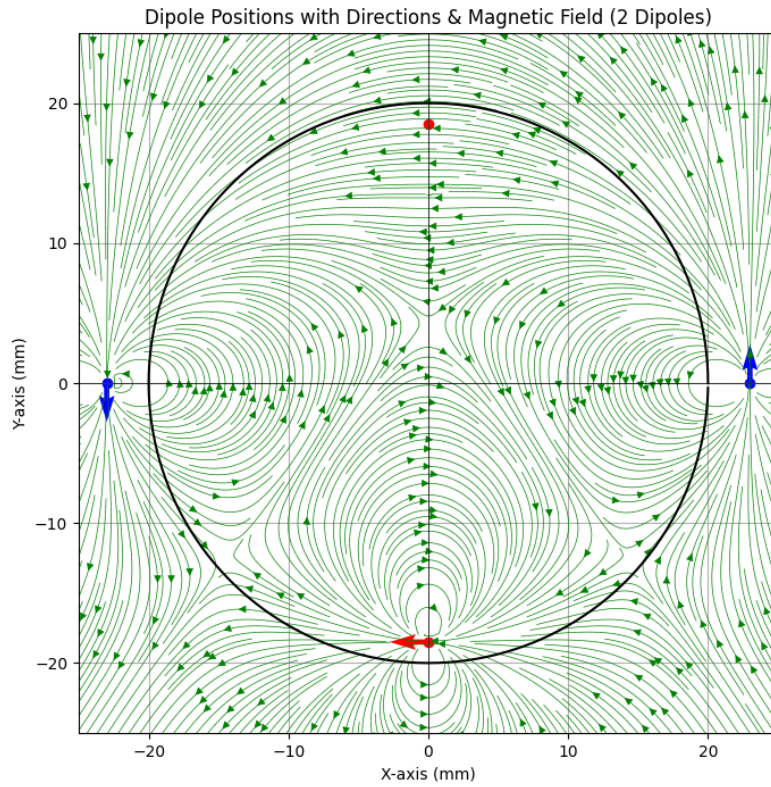


Figure 34: Simulated magnetic field with 2 dipoles.

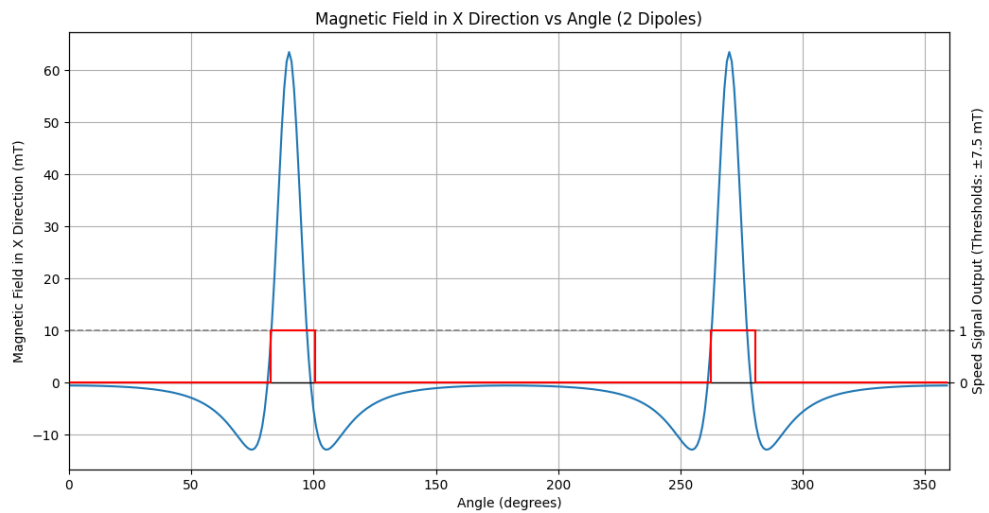


Figure 35: Simulated magnetic field along the x-plane of the Hall sensor for 2 dipoles versus angle.

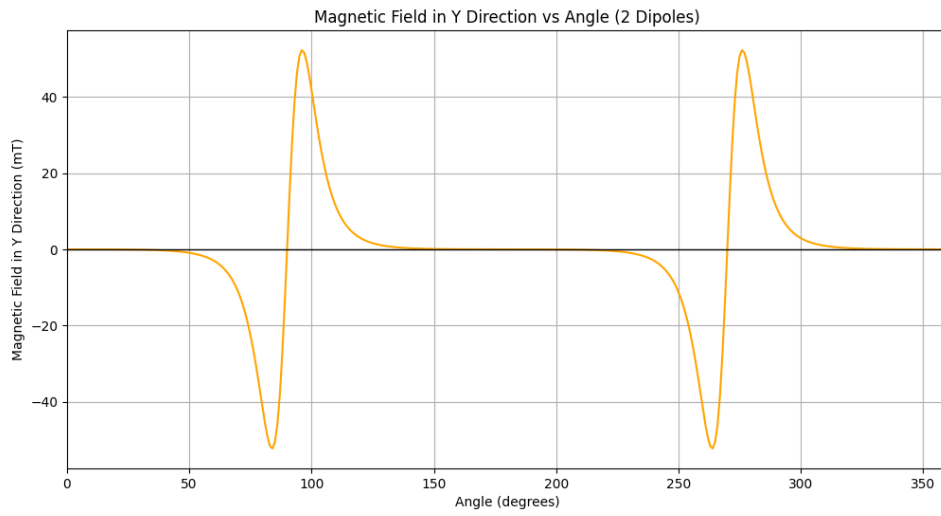


Figure 36: Simulated magnetic field along the y-plane of the Hall sensor for 2 dipoles versus angle.

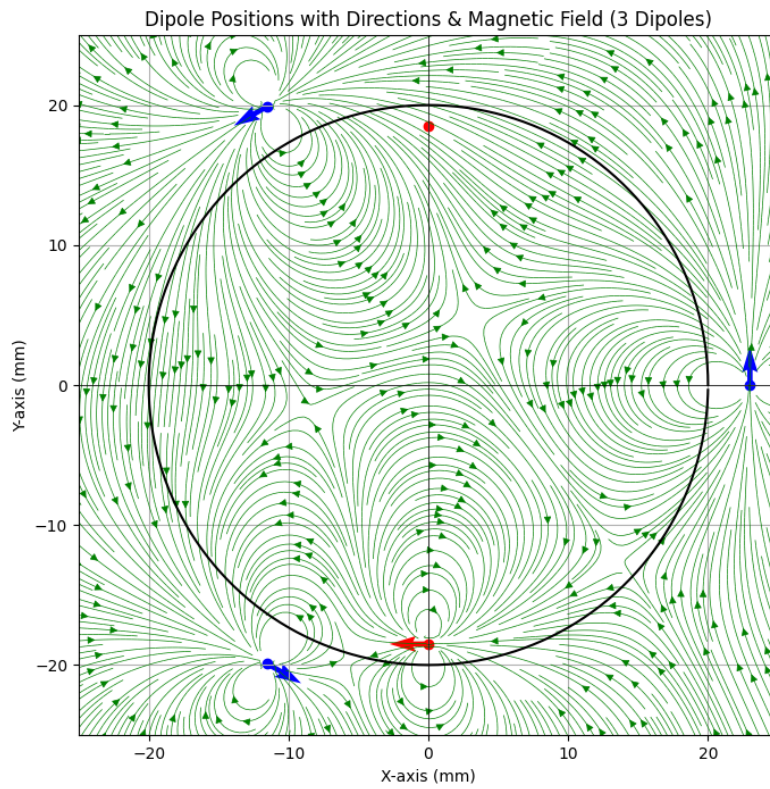


Figure 37: Simulated magnetic field with 3 dipoles.

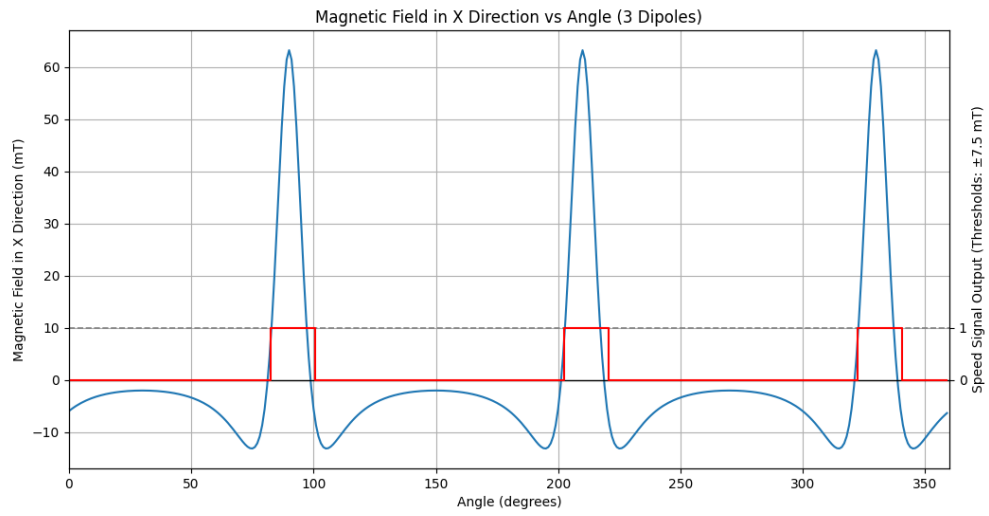


Figure 38: Simulated magnetic field along the x-plane of the Hall sensor for 3 dipoles versus angle.

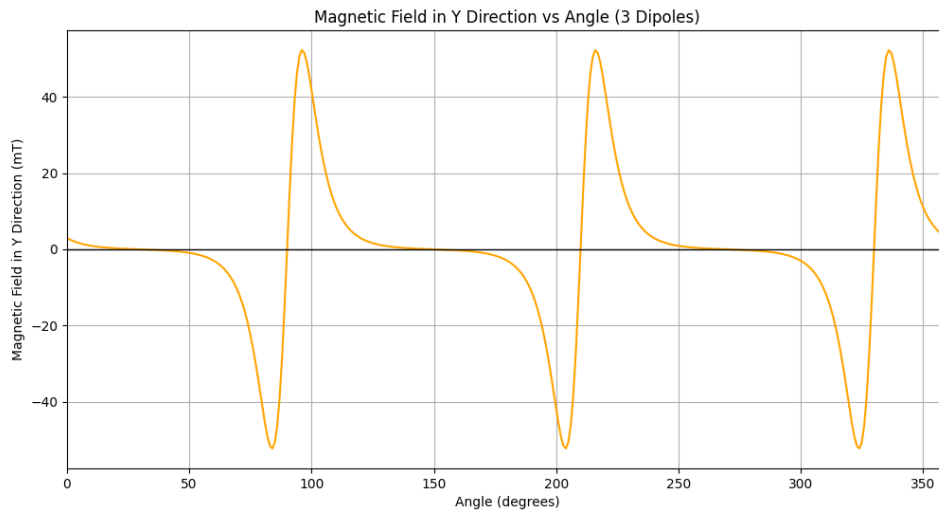


Figure 39: Simulated magnetic field along the y-plane of the Hall sensor for 3 dipoles versus angle.

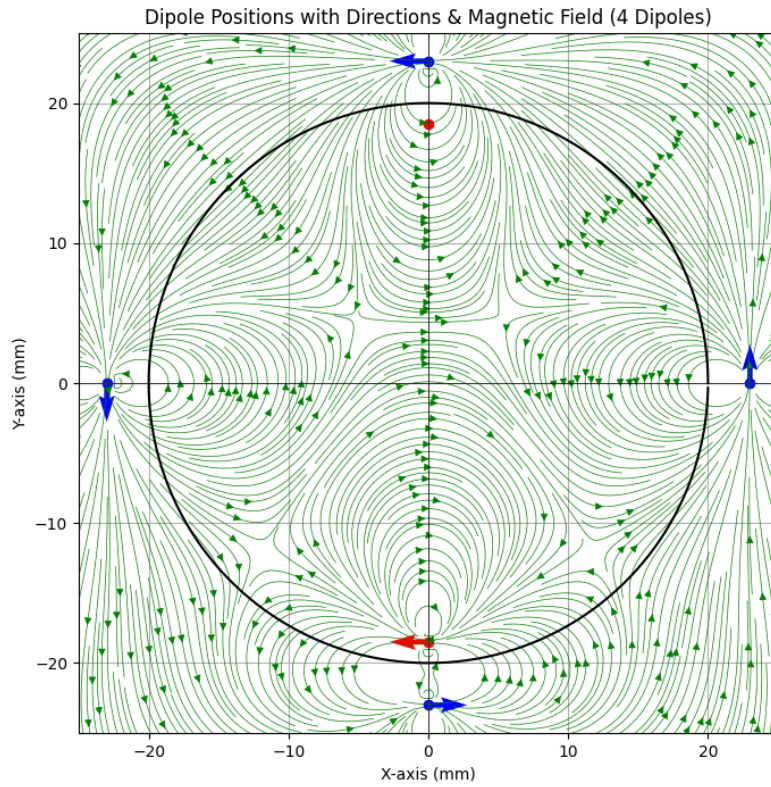


Figure 40: Simulated magnetic field with 4 dipoles.

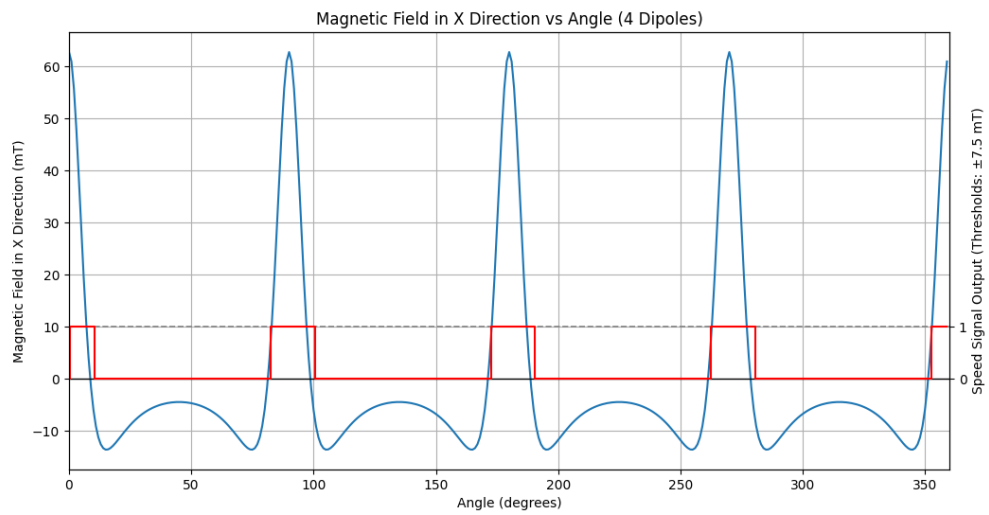


Figure 41: Simulated magnetic field along the x-plane of the Hall sensor for 4 dipoles versus angle.

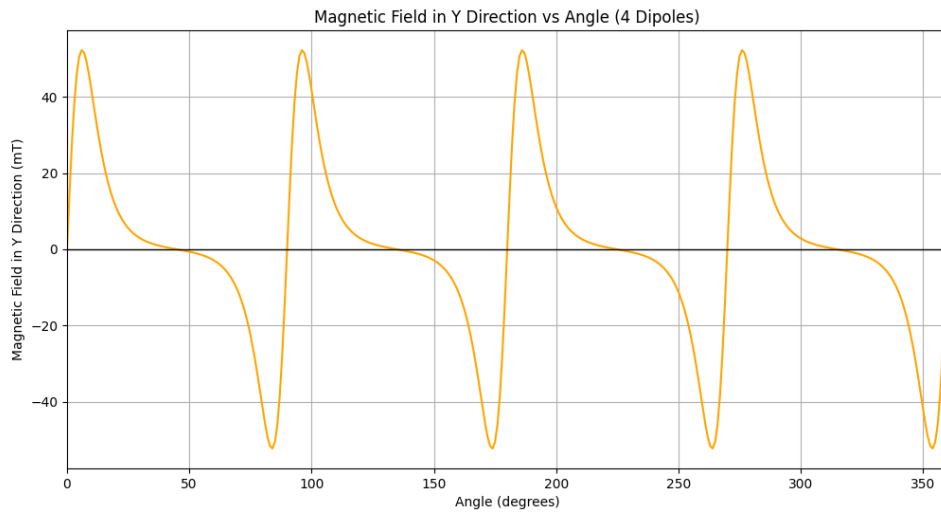


Figure 42: Simulated magnetic field along the y-plane of the Hall sensor for 4 dipoles versus angle.

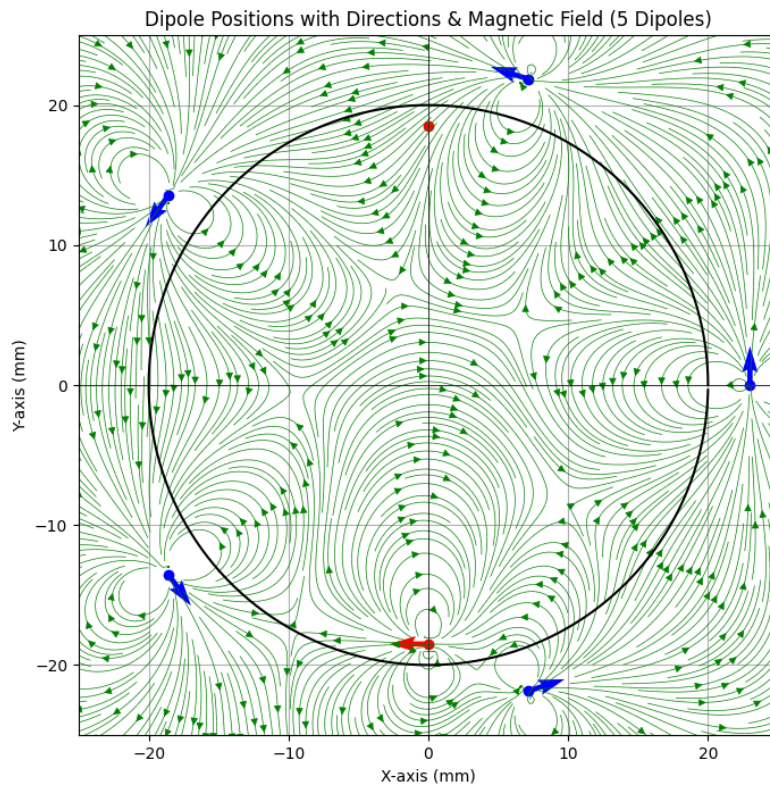


Figure 43: Simulated magnetic field with 5 dipoles.

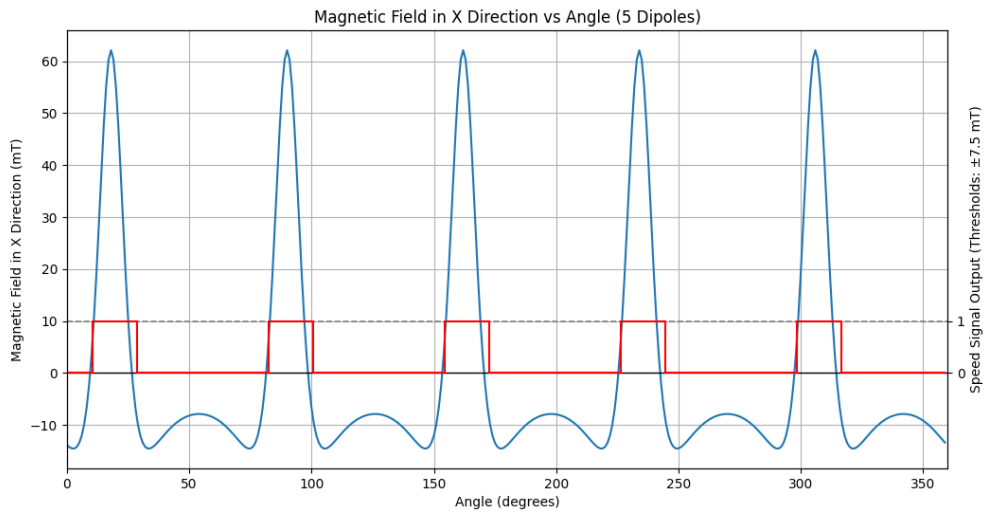


Figure 44: Simulated magnetic field along the x-plane of the Hall sensor for 5 dipoles versus angle.

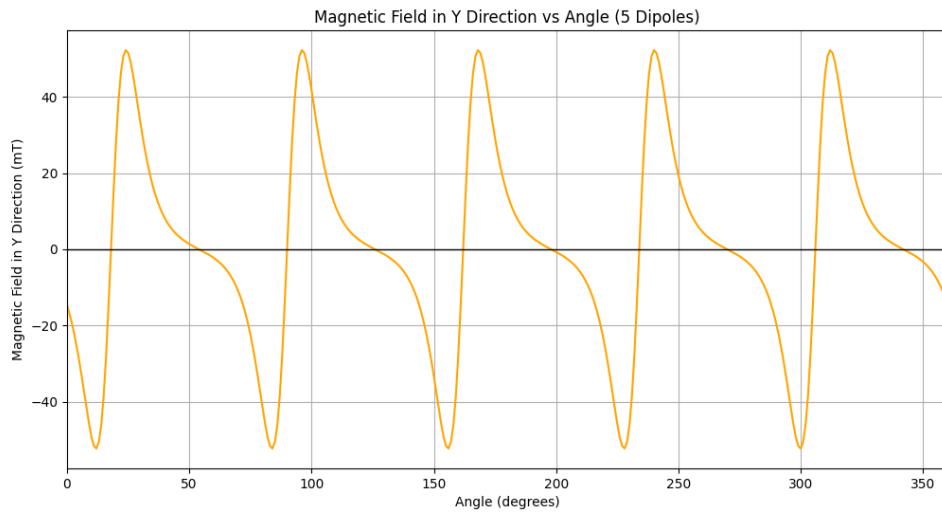


Figure 45: Simulated magnetic field along the y-plane of the Hall sensor for 5 dipoles versus angle.

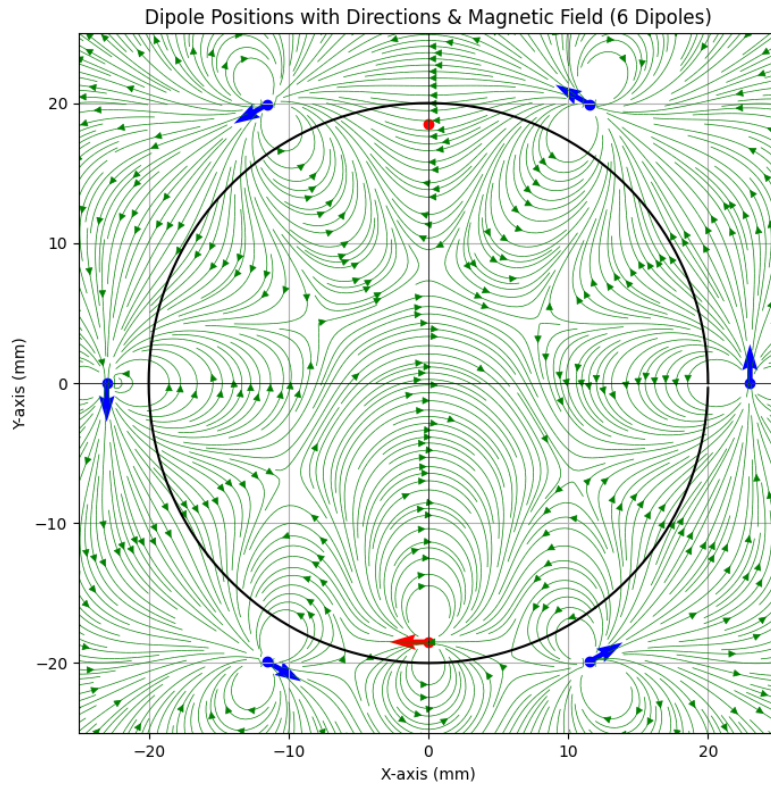


Figure 46: Simulated magnetic field with 6 dipoles.

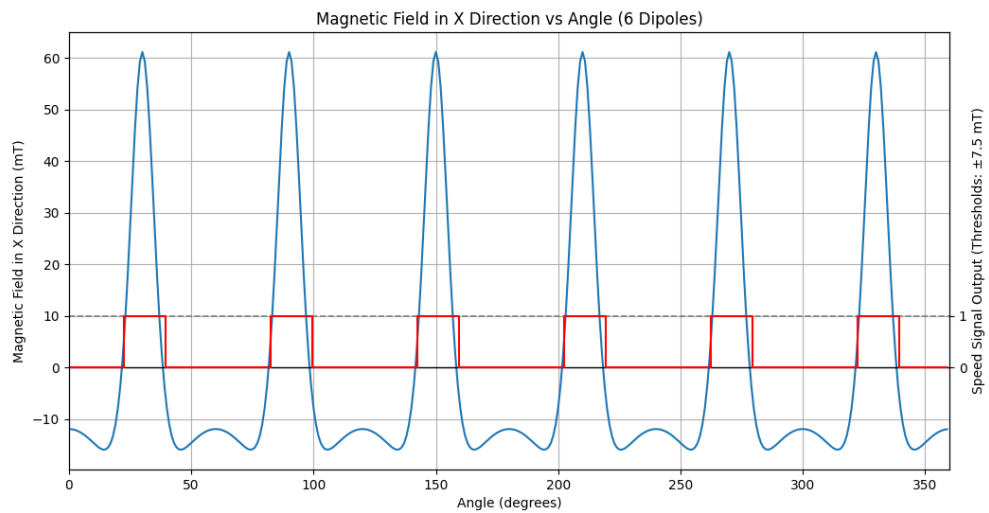


Figure 47: Simulated magnetic field along the x-plane of the Hall sensor for 6 dipoles versus angle.

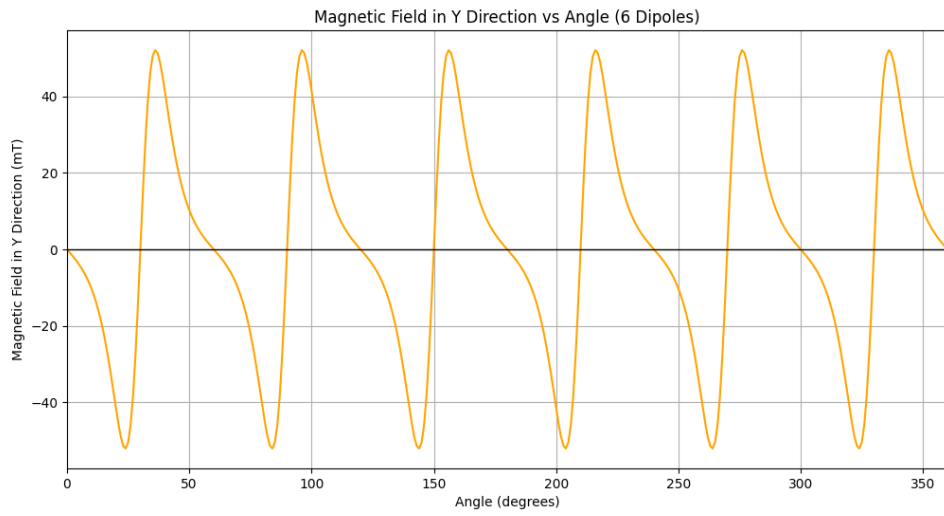


Figure 48: Simulated magnetic field along the y-plane of the Hall sensor for 6 dipoles versus angle.

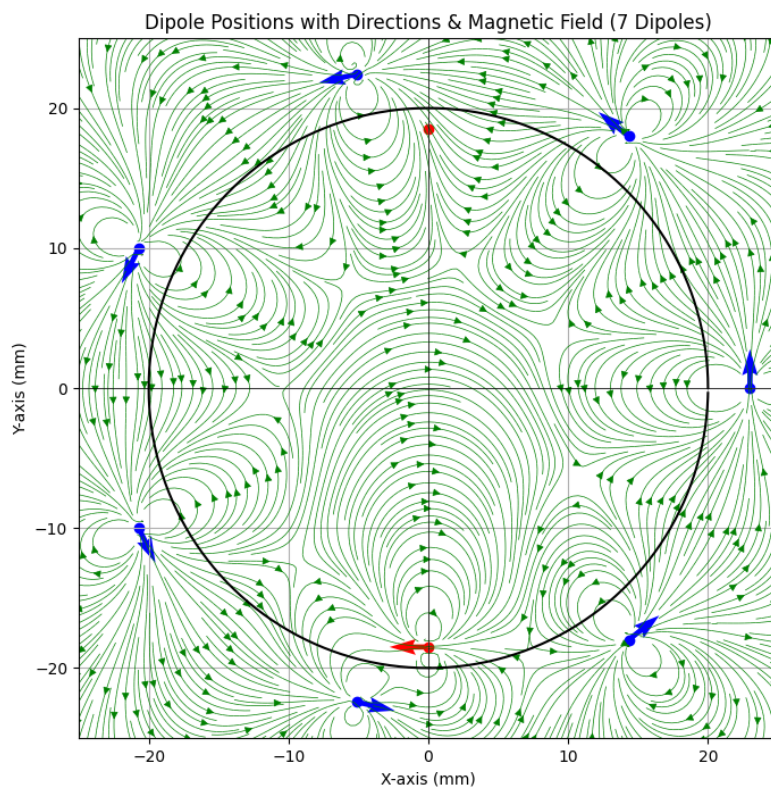


Figure 49: Simulated magnetic field with 7 dipoles.

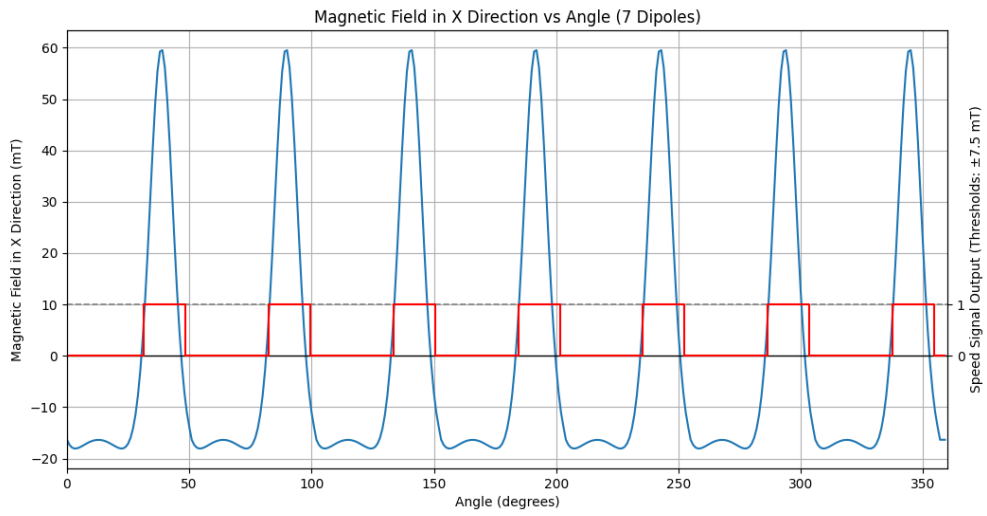


Figure 50: Simulated magnetic field along the x-plane of the Hall sensor for 7 dipoles versus angle.

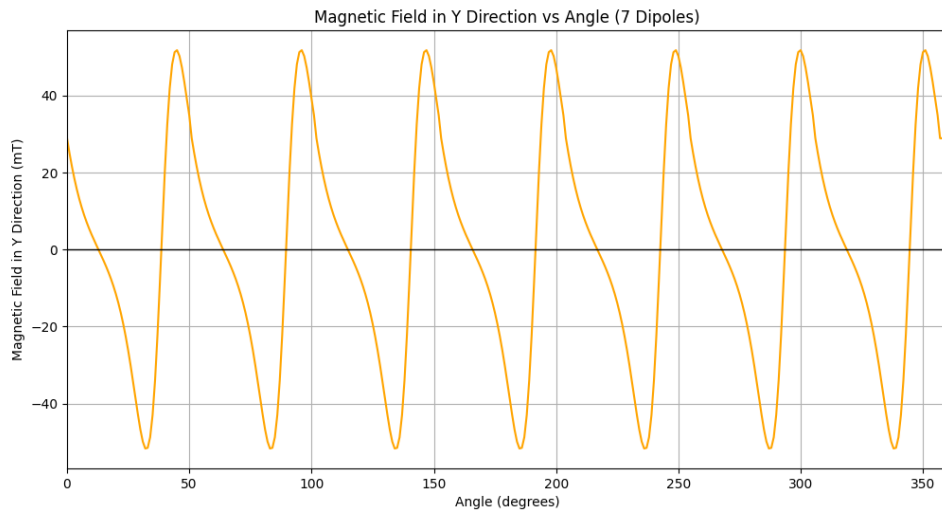


Figure 51: Simulated magnetic field along the y-plane of the Hall sensor for 7 dipoles versus angle.

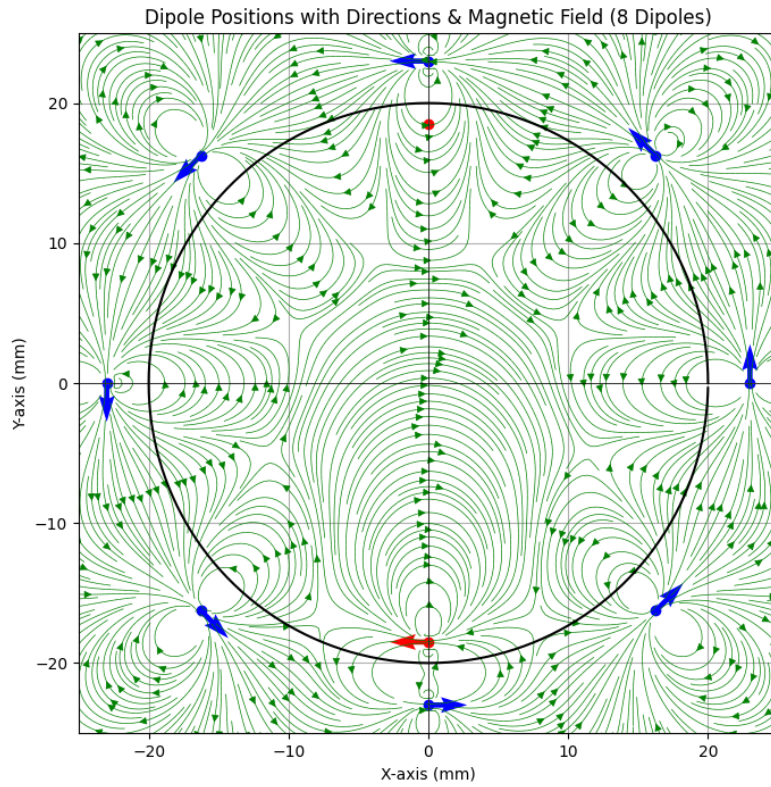


Figure 52: Simulated magnetic field with 8 dipoles.

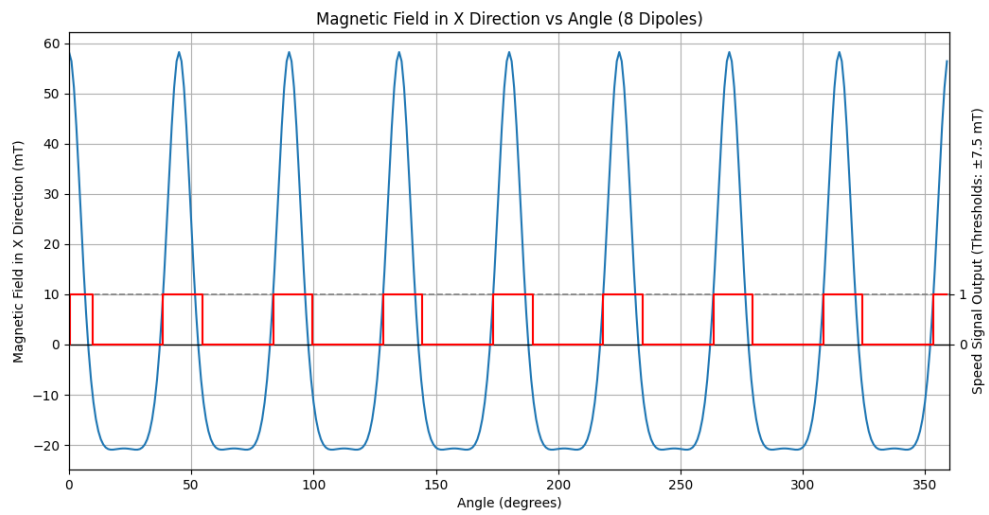


Figure 53: Simulated magnetic field along the x-plane of the Hall sensor for 8 dipoles versus angle.

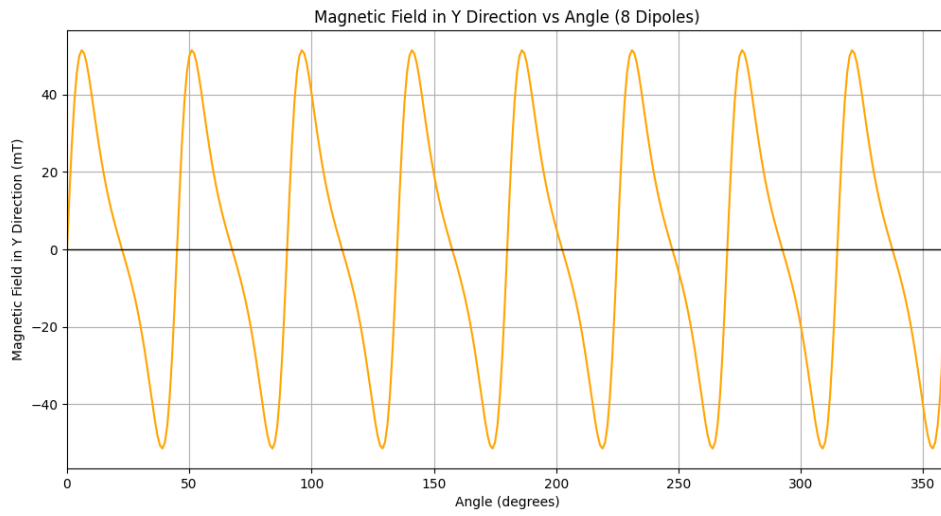


Figure 54: Simulated magnetic field along the y-plane of the Hall sensor for 8 dipoles versus angle.

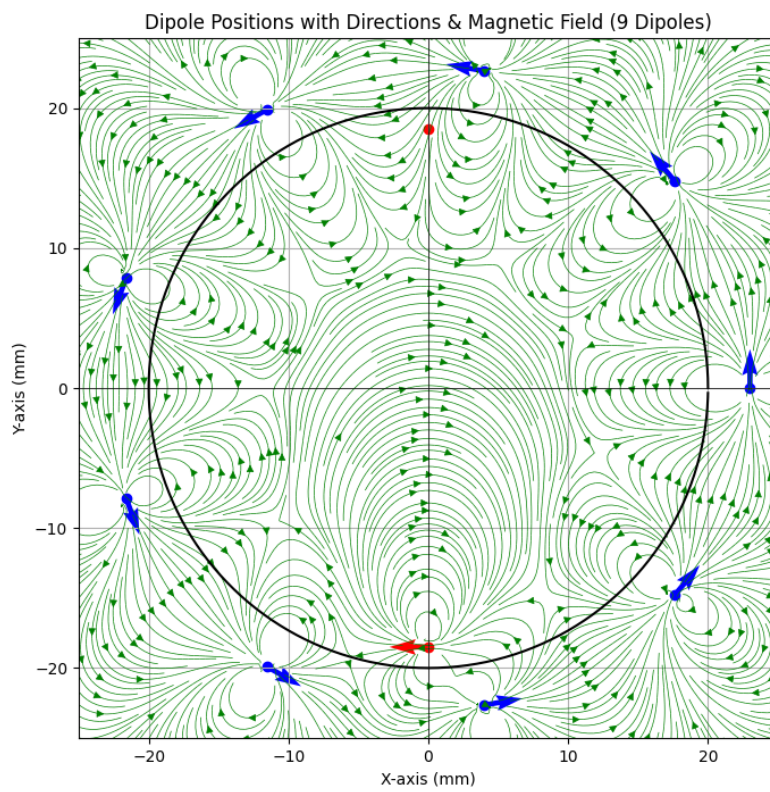


Figure 55: Simulated magnetic field with 9 dipoles.

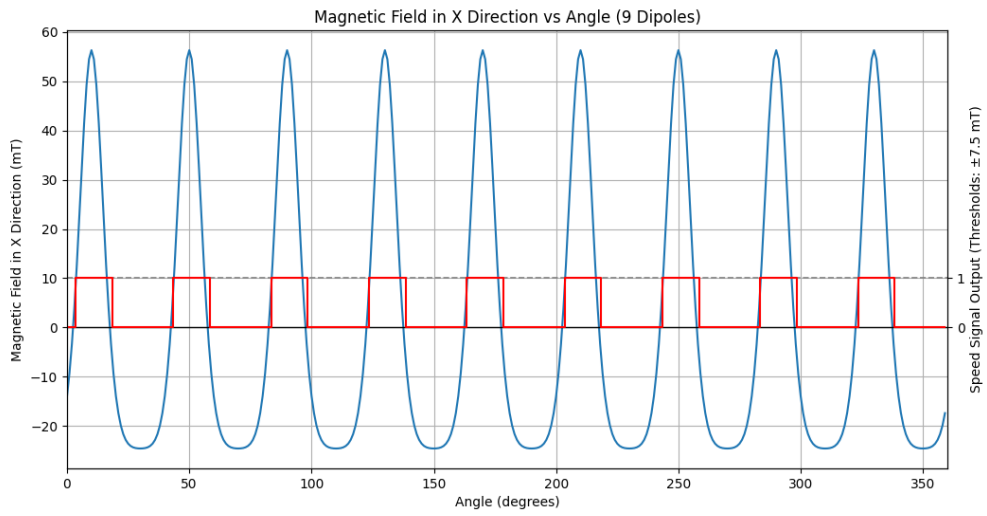


Figure 56: Simulated magnetic field along the x-plane of the Hall sensor for 9 dipoles versus angle.

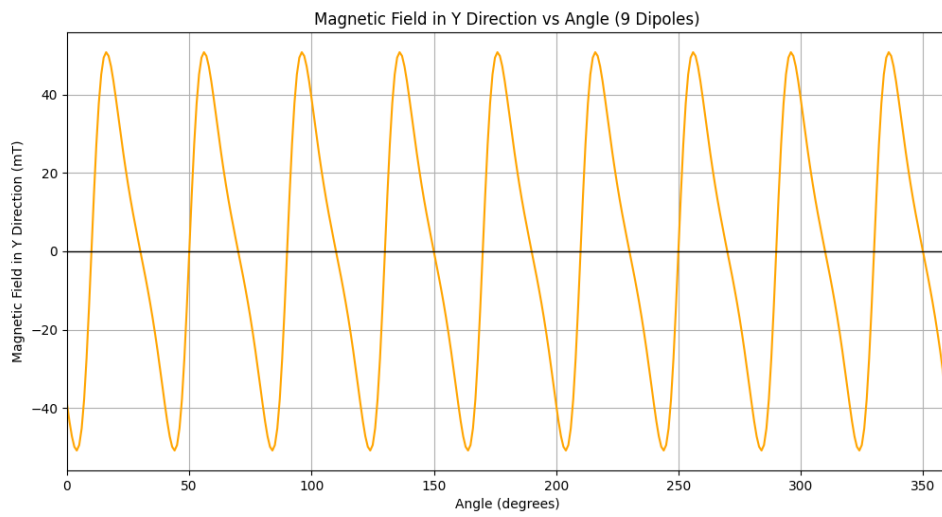


Figure 57: Simulated magnetic field along the y-plane of the Hall sensor for 9 dipoles versus angle.

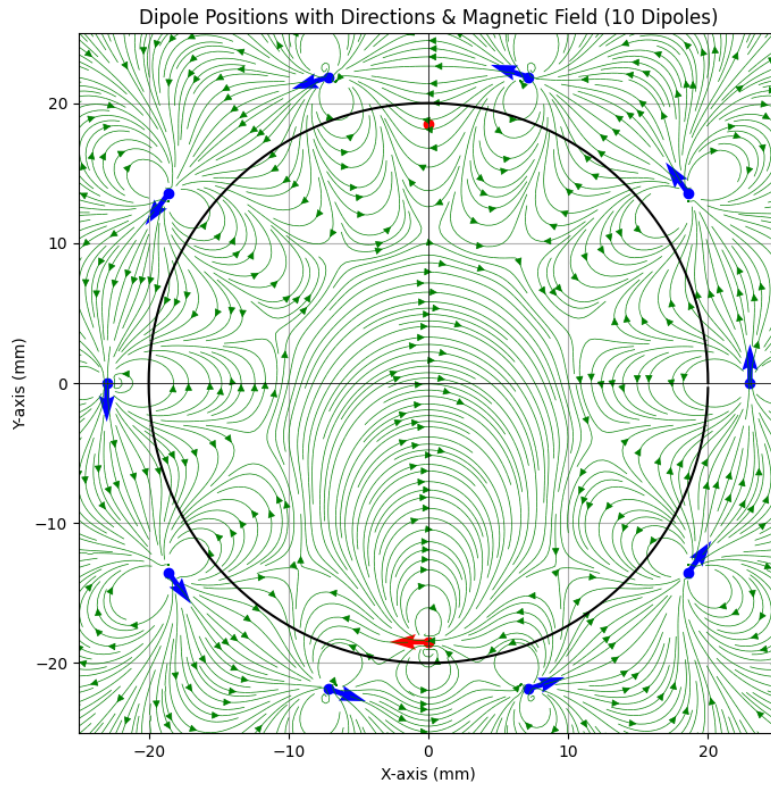


Figure 58: Simulated magnetic field with 10 dipoles.

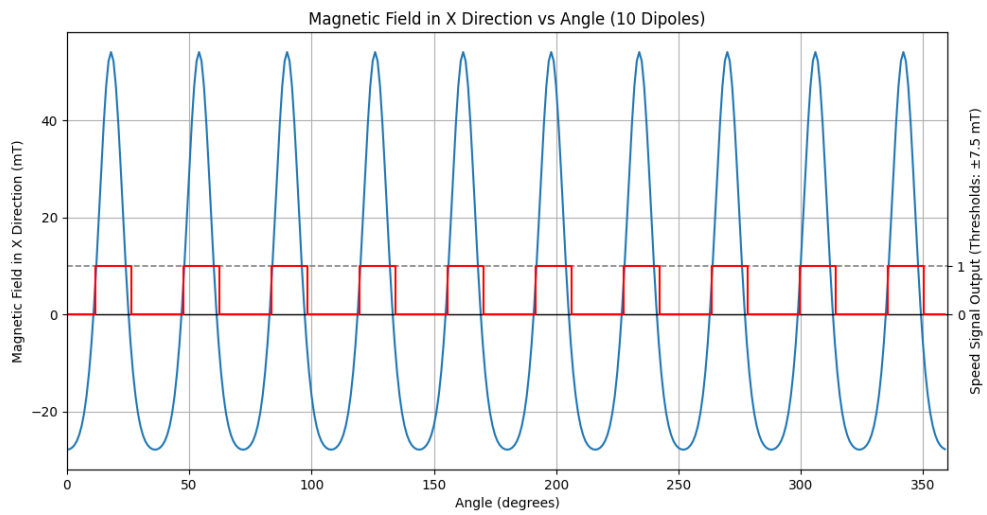


Figure 59: Simulated magnetic field along the x-plane of the Hall sensor for 10 dipoles versus angle.

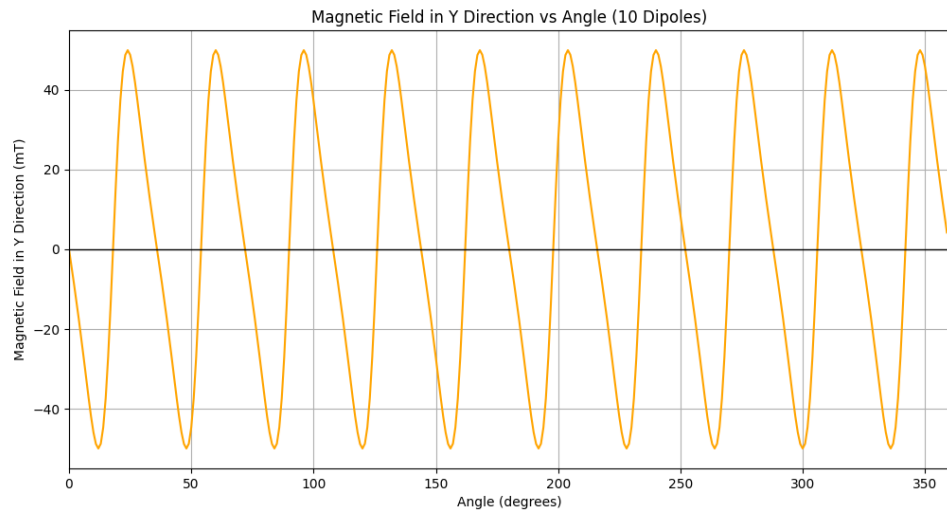


Figure 60: Simulated magnetic field along the y-plane of the Hall sensor for 10 dipoles versus angle.

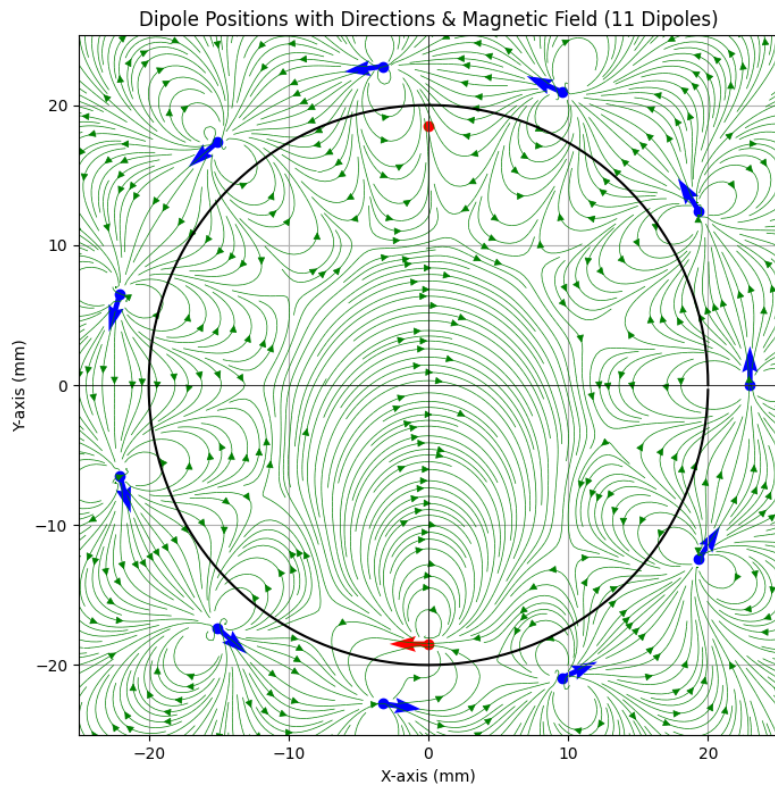


Figure 61: Simulated magnetic field with 11 dipoles.

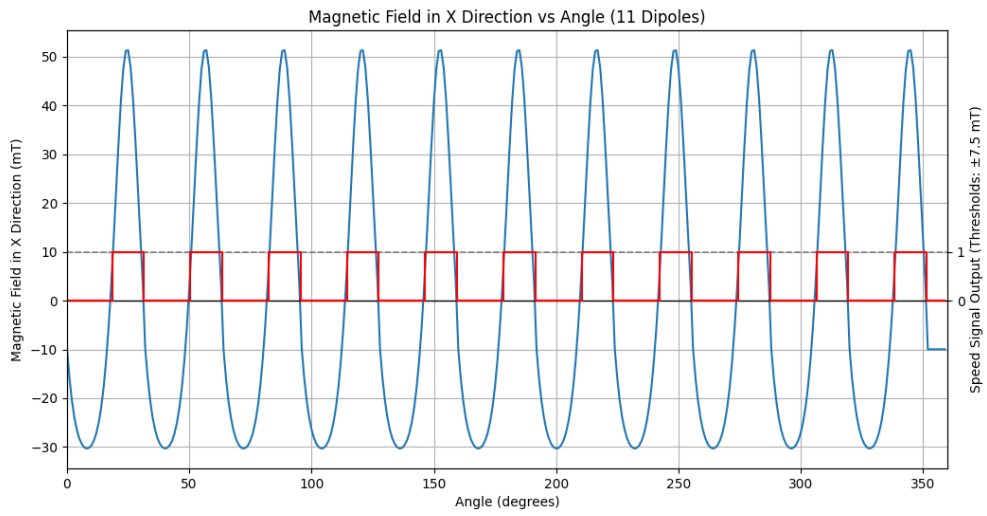


Figure 62: Simulated magnetic field along the x-plane of the Hall sensor for 11 dipoles versus angle.

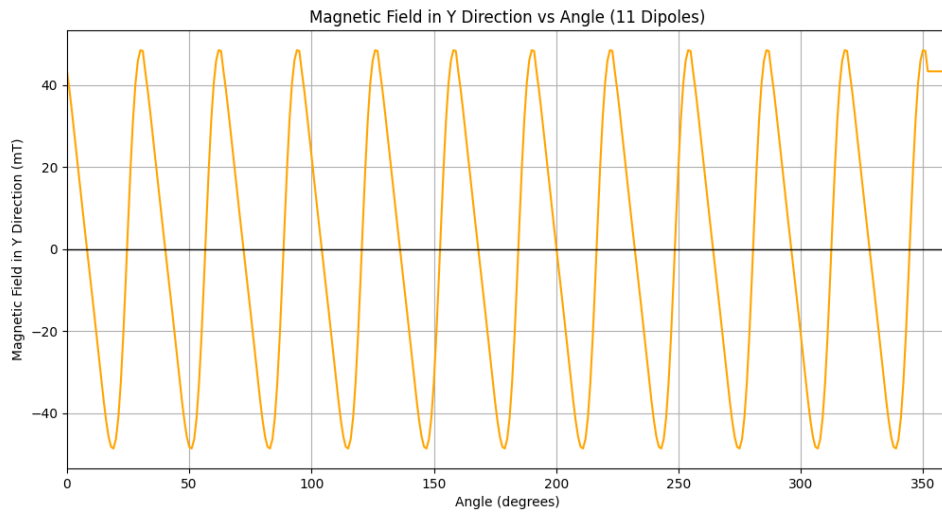


Figure 63: Simulated magnetic field along the y-plane of the Hall sensor for 11 dipoles versus angle.

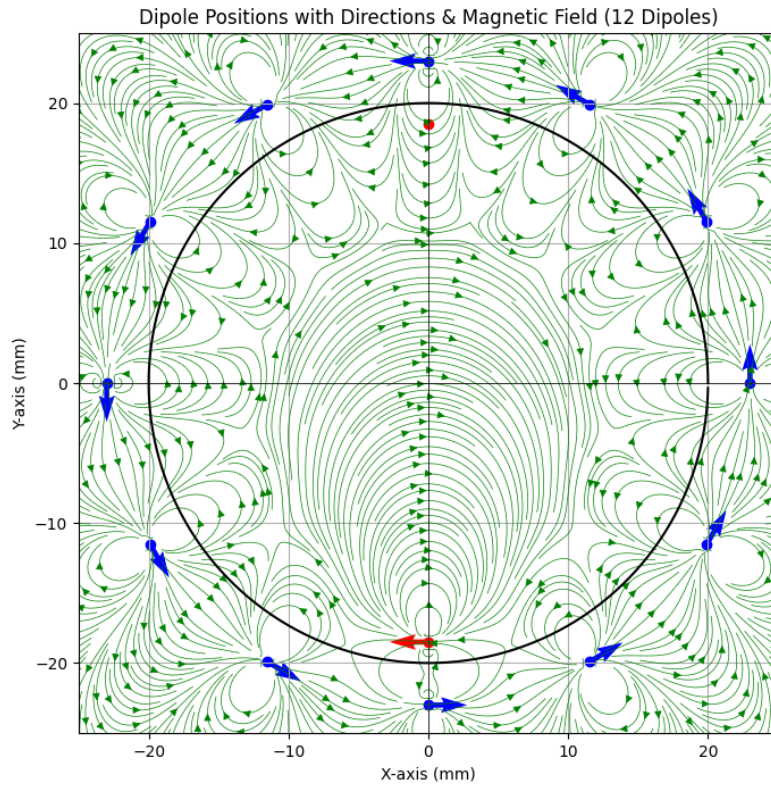


Figure 64: Simulated magnetic field with 12 dipoles.

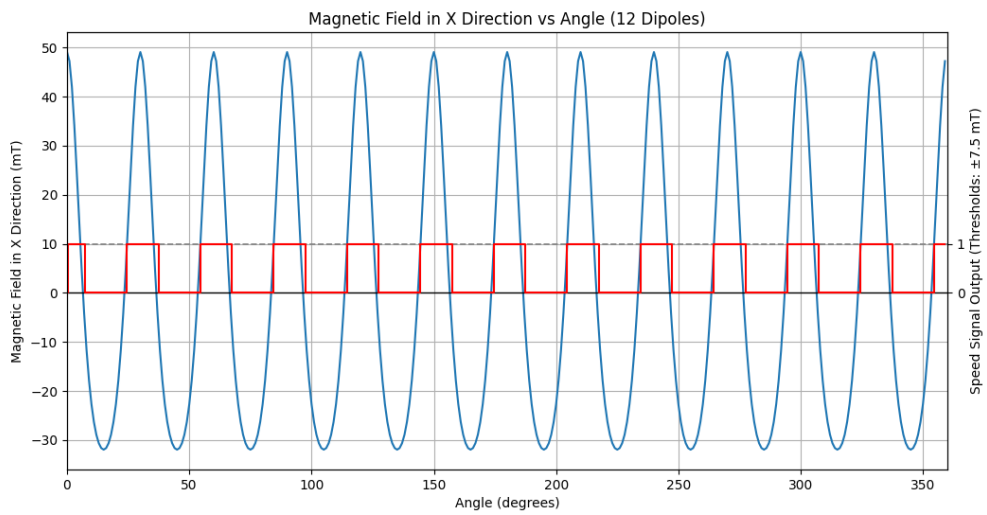


Figure 65: Simulated magnetic field along the x-plane of the Hall sensor for 12 dipoles versus angle.

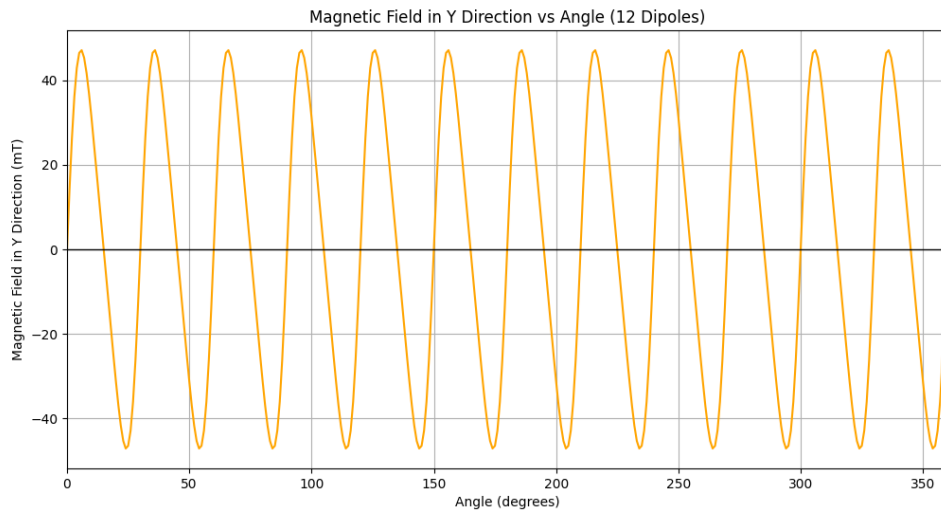


Figure 66: Simulated magnetic field along the y-plane of the Hall sensor for 12 dipoles versus angle.

D Arduino & Feather Code

D.1 Arduino code

```
1
2 int lastvalues[2] = { 0, 0 };
3 int i = 0;
4
5 // int led assignment lowest value of the pin here
6 int led = 9;
7
8 enum State {
9     idle_start,
10    idle_end,
11    turn
12 };
13
14 State current_state = idle_start;
15
16 enum Direction {
17     left,
18     right,
19     nothing
20 };
21
22 Direction direction_state = nothing;
23
24 bool buttonPressed = false;
25
26 //The setup function is called once at startup of the sketch
27 void setup() {
28     Serial.begin(115200);
29     // pin 22 = direction
30     pinMode(20, INPUT_PULLUP);
31     // pin 23 = speed
32     pinMode(21, INPUT_PULLUP);
33     // button
34     pinMode(12, INPUT_PULLUP);
35
36     pinMode(led, OUTPUT);
37     pinMode(led + 1, OUTPUT);
38     pinMode(led + 2, OUTPUT);
39
40     digitalWrite(led, HIGH);
41 }
42
43 // The loop function is called in an endless loop
44 void loop() {
45     int direction = digitalRead(21);
46     int speed = digitalRead(20);
47
48     int pinState = digitalRead(12);
49
50     int pinState4 = digitalRead(led);
51     int pinState5 = digitalRead(led + 1);
52     int pinState6 = digitalRead(led + 2);
53
54
55     // Check if the button is pressed
56     if (pinState == HIGH) { // Assuming LOW means the button is pressed
```

```

57     buttonPressed = true;
58     // Turn all LEDs on
59     digitalWrite((i % 3) + led, HIGH);
60     delay(250);
61     digitalWrite((i % 3) + led, LOW);
62     delay(250);
63
64     lastvalues[0] = direction;
65     lastvalues[1] = speed;
66
67     // Do not send any data
68     return;
69 } else {
70     buttonPressed = false;
71 }
72
73
74 if(!buttonPressed){
75     switch (direction_state) {
76         case left:
77             Serial.println("left")
78             --i;
79             break;
80         case right:
81             Serial.println("right")
82             ++i;
83             break;
84         case nothing:
85             break;
86     }
87
88     if (direction == lastvalues[0]) {
89         switch (current_state) {
90             case idle_start:
91                 direction_state = nothing;
92                 if (speed == lastvalues[1]) {
93                     current_state = idle_start;
94                 } else {
95                     current_state = turn;
96                 }
97                 break;
98             case turn:
99                 if (direction == 1) {
100                     direction_state = left;
101                 } else if (direction == 0) {
102                     direction_state = right;
103                 }
104                 else {
105                     direction_state = nothing;
106                 }
107
108                 current_state = idle_end;
109                 break;
110             case idle_end:
111                 direction_state = nothing;
112                 if (speed == lastvalues[1]) {
113                     current_state = idle_end;
114                 } else {
115                     current_state = idle_start;
116                 }
117                 break;

```

```

118     }
119 }
120
121 else {
122     if (direction == 1) {
123         direction_state = left;
124     } else {
125         direction_state = right;
126     }
127 }
128
129 // direction, speed
130 lastvalues[0] = direction;
131 lastvalues[1] = speed;
132
133 digitalWrite(led, LOW);
134 digitalWrite(led + 1, LOW);
135 digitalWrite(led + 2, LOW);
136
137 if (i % 3 < 0) {
138     i += 3;
139 }
140
141 digitalWrite((i % 3) + led, HIGH);
142 // delay(50);
143 }
144 delay(100);
145 }

```

D.2 Feather Code

```

1  #include <SPI.h>
2  #include <RH_RF69.h>
3
4  // Singleton instance of the radio driver
5  RH_RF69 rf69(8, 7); // Adafruit Feather 32u4
6
7  void setup_RF69() {
8      if (!rf69.init()) {
9          while (1) {
10             digitalWrite(LED_BUILTIN, HIGH);
11             delay(500);
12             digitalWrite(LED_BUILTIN, LOW);
13             delay(500);
14         }
15     }
16     digitalWrite(LED_BUILTIN, HIGH);
17
18     // ISM frequency, in MHz
19     if (!rf69.setFrequency(868.0)) {
20         digitalWrite(LED_BUILTIN, LOW);
21     }
22
23     // The encryption key has to be the same as the one in the client
24     rf69.setEncryptionKey((uint8_t*)"thisIsEncryptKey");
25 }
26
27 int lastvalues[2] = { 0, 0 };

```

```

28
29 // int array[3] = {2, 3, 4}; //staat er 1 keer in word niet gebruikt
30 int i = 0;
31 // int led assignment lowest value of the pin here
32 int led = 9;
33
34 enum State {
35     idle_start,
36     idle_end,
37     turn
38 };
39
40 State current_state = idle_start;
41
42 enum Direction {
43     left,
44     right,
45     nothing
46 };
47
48 Direction direction_state = nothing;
49
50 bool buttonPressed = false;
51
52 //The setup function is called once at startup of the sketch
53 void setup() {
54     Serial.begin(115200);
55     setup_RF69();
56     // pin 18 = direction
57     pinMode(22, INPUT_PULLUP);
58     // pin 19 = speed
59     pinMode(23, INPUT_PULLUP);
60     // button
61     pinMode(12, INPUT_PULLUP);
62
63     pinMode(led, OUTPUT);
64     pinMode(led + 1, OUTPUT);
65     pinMode(led + 2, OUTPUT);
66
67     digitalWrite(led, HIGH);
68 }
69
70 // The loop function is called in an endless loop
71 void loop() {
72     int direction = digitalRead(23);
73     int speed = digitalRead(22);
74
75     int pinState = digitalRead(12);
76
77     int pinState4 = digitalRead(led);
78     int pinState5 = digitalRead(led + 1);
79     int pinState6 = digitalRead(led + 2);
80
81
82     // Check if the button is pressed
83     if (pinState == HIGH) { // Assuming LOW means the button is pressed
84         buttonPressed = true;
85         // Turn all LEDs on
86         digitalWrite((i % 3) + led, HIGH);
87         delay(250);
88         digitalWrite((i % 3) + led, LOW);

```

```

89     delay(250);
90
91     lastvalues[0] = direction;
92     lastvalues[1] = speed;
93
94     // Do not send any data
95     return;
96 } else {
97     buttonPressed = false;
98 }
99
100
101 if(!buttonPressed){
102     switch (direction_state) {
103         case left:
104             rf69.send("left", sizeof("left"));
105             rf69.waitPacketSent();
106             --i;
107             break;
108         case right:
109             rf69.send("right", sizeof("right"));
110             rf69.waitPacketSent();
111             ++i;
112             break;
113         case nothing:
114             break;
115     }
116
117     if (direction == lastvalues[0]) {
118         switch (current_state) {
119             case idle_start:
120                 direction_state = nothing;
121                 if (speed == lastvalues[1]) {
122                     current_state = idle_start;
123                 } else {
124                     current_state = turn;
125                 }
126                 break;
127             case turn:
128                 if (direction == 1) {
129                     direction_state = left;
130                 } else if (direction == 0) {
131                     direction_state = right;
132                 }
133                 else {
134                     direction_state = nothing;
135                 }
136
137                 current_state = idle_end;
138                 break;
139             case idle_end:
140                 direction_state = nothing;
141                 if (speed == lastvalues[1]) {
142                     current_state = idle_end;
143                 } else {
144                     current_state = idle_start;
145                 }
146                 break;
147         }
148     }
149

```

```

150     else {
151         if (direction == 1) {
152             direction_state = left;
153         } else {
154             direction_state = right;
155         }
156     }
157
158     // direction, speed
159     lastvalues[0] = direction;
160     lastvalues[1] = speed;
161
162     digitalWrite(led, LOW);
163     digitalWrite(led + 1, LOW);
164     digitalWrite(led + 2, LOW);
165
166     if (i % 3 < 0) {
167         i += 3;
168     }
169
170     digitalWrite((i % 3) + led, HIGH);
171     // delay(50);
172     }
173     delay(100);
174 }

```

D.3 Feather Receiver Code

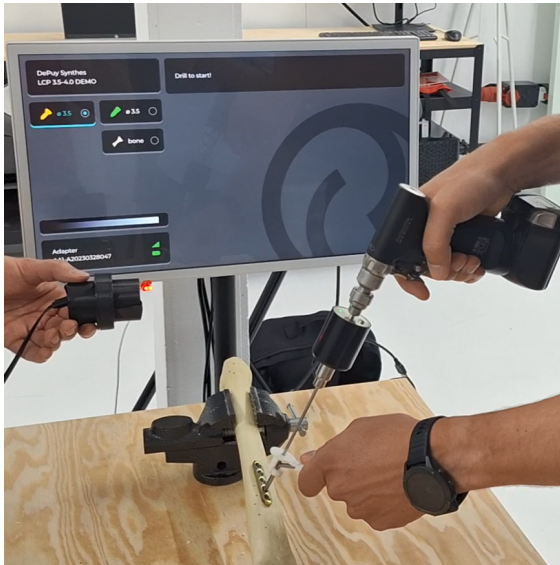
```

1  #include <SPI.h>
2  #include <RH_RF69.h>
3
4  // Singleton instance of the radio driver
5  RH_RF69 rf69(8, 7); // Adafruit Feather 32u4
6
7  void setup(){
8      Serial.begin(9600);
9      while (!Serial) ;
10     if (!rf69.init()){
11         Serial.println("init failed");
12         while (1){
13             digitalWrite(LED_BUILTIN, HIGH);
14             delay(500);
15             digitalWrite(LED_BUILTIN, LOW);
16             delay(500);
17         }
18     }
19     Serial.println("RFM69 radio init OK!");
20     digitalWrite(LED_BUILTIN, HIGH);
21
22     // ISM frequency, in MHz
23     if (!rf69.setFrequency(868.0)){
24         Serial.println("setFrequency failed");
25         digitalWrite(LED_BUILTIN, LOW);
26     }
27
28     // The encryption key has to be the same as the one in the client
29     rf69.setEncryptionKey((uint8_t*)"thisIsEncryptKey");
30 }

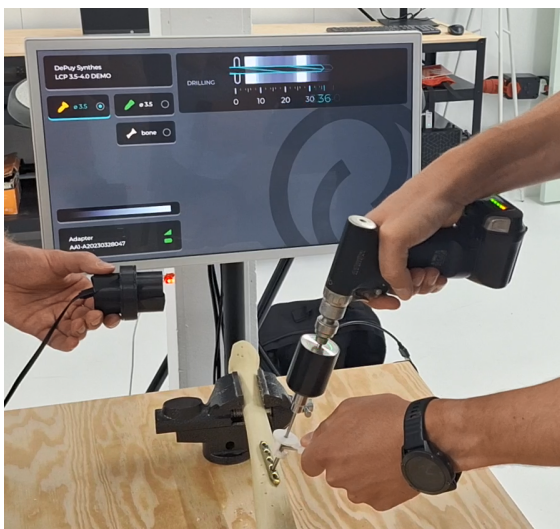
```

```
31
32 void loop(){
33     if (rf69.available()){
34         // Should be a message for us now
35         uint8_t buf[RH_RF69_MAX_MESSAGE_LEN];
36         uint8_t len = sizeof(buf);
37         if (rf69.recv(buf, &len)){
38             // RH_RF69::printBuffer("request: ", buf, len);
39             Serial.print("Got message: ");
40             Serial.println((char*)buf);
41         }
42     }
43 }
```


E Prototype Results



(a) Start of the drilling process.



(b) Drilling into the bone.



(c) First hole has been drilled.

Description: This is where the drilling procedure starts. The orthopedic surgeon starts by choosing the first screw type, which is the orange cortical screw.

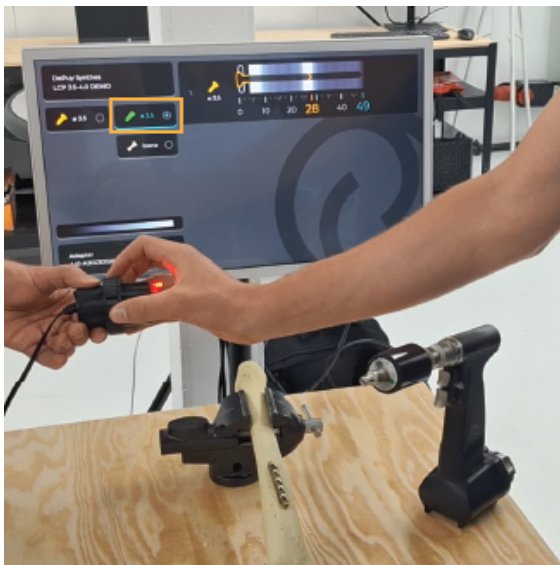
Description: The Orthopedic surgeon starts by drilling into the bone. The screen shows in real-time how far the surgeon has drilled into the bone.

Description: Once the surgeon drilled fully through the bone, the screen shows the final length of the screw. The length of the screw should be 28mm for the orange (cortical) screw, as shown on screen.



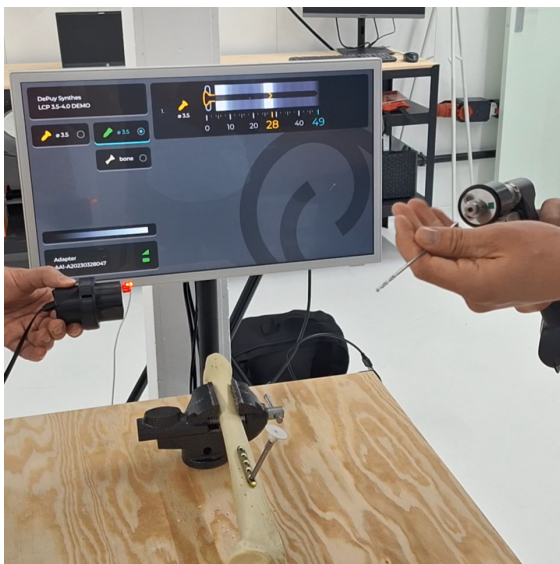
(d) The drill bit for the cortical screw type is taken off the drill.

Description: The drill bit is replaced with a screw bit to screw in the orange cortical screw, which has a length of 28 mm. The surgeon then screws in that length and type of screw, this was not a part of the demo so this was not done. The orange square shows that the cortical screw type is selected.



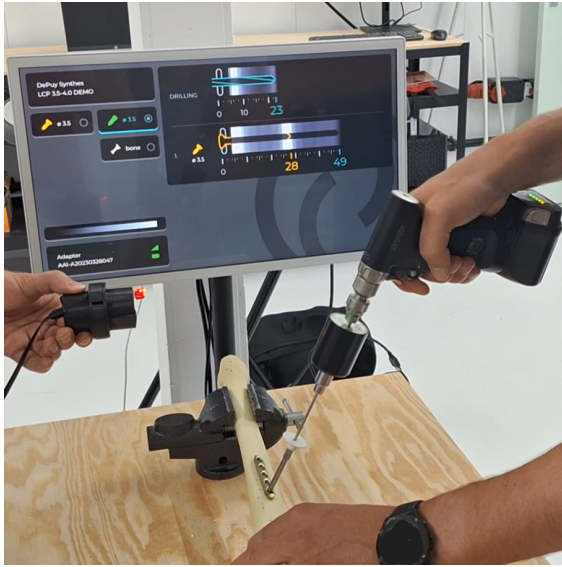
(e) The next screw type is selected with rotating the ring.

Description: The surgeon, after screwing in the correct screw, selects the next screw type by rotating the ring to the desired screw type. The next screw type is the green locking screw. The orange rectangle in Figure 67e shows that the locking screw is selected instead of the cortical in Figure 67d.



(f) The correct drill bit is put on the drill.

Description: The surgeon places the drill bit corresponding to the selected screw type onto the drill.



(g) Drilling the hole for the green screw type.

Description: When the drill is used and the ADEPTH starts rotating, the locking screw is chosen. The surgeon starts drilling the hole for the locking screw.



(h) The second hole has been drilled.

Description: The second hole has a depth of 31mm, after drilling the hole. The surgeon then places a locking screw of 31mm. The drilling procedure is finished.

Figure 67: Demonstration on how the rotary switch would be used during an operation.